

Symbolic Approximations to Ricci-flat Metrics Via Extrinsic Symmetries of Calabi–Yau Hypersurfaces

Viktor Mirjanić and Challenger Mishra

Department of Computer Science and Technology, University of Cambridge

E-mail: vvm22@cam.ac.uk, cm2099@cam.ac.uk

ABSTRACT: Ever since Yau’s non-constructive existence proof of Ricci-flat metrics on Calabi–Yau manifolds, finding their explicit construction remains a major obstacle to development of both string theory and algebraic geometry. Recent computational approaches employ machine learning to create novel neural representations for approximating these metrics, offering high accuracy but limited interpretability. In this paper, we analyse machine learning approximations to flat metrics of Fermat Calabi–Yau n -folds and some of their one-parameter deformations in three dimensions in order to discover their new properties. We formalise cases in which the flat metric has more symmetries than the underlying manifold, and prove that these symmetries imply that the flat metric admits a surprisingly compact representation for certain choices of complex structure moduli. We show that such symmetries uniquely determine the flat metric on certain loci, for which we present an analytic form. We also incorporate our theoretical results into neural networks to achieve state-of-the-art reductions in Ricci curvature for multiple Calabi–Yau manifolds. We conclude by distilling the ML models to obtain for the first time closed form expressions for Kähler metrics with near-zero scalar curvature.

Contents

1	Introduction	2
2	Background and Related Work	3
2.1	Machine Learning	3
2.2	Calabi–Yau Manifolds	4
2.3	Machine Learning Ricci-flat Metrics	5
2.4	Explainable AI	7
3	Symmetric Forms on Calabi–Yaus	8
3.1	Permutation Symmetry of Calabi–Yaus	8
3.2	Saliency of Symmetric Features	10
3.3	Extrinsic Symmetries of Calabi–Yau Hypersurfaces	12
4	Neural Network Approximations to ϕ	13
4.1	The Fermat Family	14
4.1.1	Machine Learning ϕ with ModNet	15
4.2	The 0–1 Mixed Family	18
4.3	The Dwork Family	19
5	Symbolic Approximations to ϕ	20
5.1	Compressing Distilled Expressions	22
5.2	Towards the Root of the Problem	22
6	Analytical Properties of ϕ	24
6.1	Exact Formulae for the Flat Metric	27
7	Discussion	28
A	Theorem Proofs	30
B	Low Loss Coefficients	32
C	Generating Interpretable Formulae with PySR	33
D	Feature Attribution on the Quintic	33
E	Second Order Differentiation Lemma	34

1 Introduction

Since the last century, algebraic geometry has been closely tied to modern physics via string theory in an attempt to unify gravity and quantum mechanics. One of the major open problems, relevant to both algebraic geometry and superstring theory, involves the study of Ricci-flat metrics on Calabi–Yau varieties. The seminal Calabi–Yau theorem [1] states that these manifolds possess a unique flat metric in each Kähler class. This metric is essential for computing phenomenological quantities, such as particle masses and physical Yukawa couplings in the context of Calabi–Yau compactifications of the heterotic string, but an explicit construction for it has not been found yet.

In this paper we do not focus on these downstream uses of Ricci-flat metrics. Instead, we make finding them less challenging, as very little is known about them in the first place. There exists an algorithm to compute them due to Donaldson [2], but it suffers from the curse of dimensionality. Neural networks perform much better, but have other issues such as lack of convergence guarantees (see Section 2.3 and [3] for a more detailed discussion). We show that the neural network outputs can be analysed to yield new properties of the flat metric and its symmetries.

Studying symmetries of families of Calabi–Yaus has long been a fruitful endeavour yielding many interesting results. One remarkable observation with many far-reaching consequences for string theory and for algebraic geometry is the mirror symmetry of Candelas et al. [4] that relates Calabi–Yaus with their mirror pairs. On the other hand, one can study symmetries of a single manifold via its isometry group. These symmetry groups have been extensively studied [5, 6, 7, 8, 9, 10, 11], often in the context of building string vacua that recover the standard model of particle physics. In three complex dimensions, such symmetries are discrete and can improve understanding of a myriad phenomenological issues that arise when connecting string theory to four dimensional particle physics [12], such as proton decay (by studying R symmetries) and Wilson line breaking for gauge unification. They can also help in explaining the structure of flavour mixing matrices such as CKM and PMNS [13] and in studying anomaly cancellation [14]. Furthermore, one can quotient the manifolds by free group actions to obtain new Calabi–Yaus with different topological properties for string compactification [10, 15, 16, 17, 18].

Our contributions are that we look at extensions of $(0,0)$ -forms on Calabi–Yau hypersurfaces to the ambient space \mathbb{P}^n in order to describe cases in which flat metrics have representations with additional symmetries that were not previously considered.

These symmetries are separate from the symmetries of the underlying Calabi–Yaus, and they can be continuous even if the Calabi–Yau only has discrete symmetries. There are no theoretical obstructions to this since these symmetries exist only in the ambient space. Thus, for example, the vanishing of the Killing vector field for some Calabi–Yaus only implies non-existence of continuous symmetries on the Calabi–Yau itself, but says nothing about these *extrinsic* symmetries that we introduce with our paper.

We show that these additional symmetries strongly constrain the flat metric. This results in easier training of neural networks, and improves upon similar observations first made in [19]. It also allows for distillation into compact closed form expressions without increase in

loss. One major issue with ML approximated flat metrics is that certain constraints, such as positivity, are often only softly enforced. By distilling ML models into closed form we circumvent many downsides such as this, allowing them to be directly checked if needed. Finally, the symmetry conditions we identify are strong enough that there emerge non-trivial loci on the Calabi–Yaus, on which the flat metric becomes completely determined.

The outline of the paper is as follows. In Section 2 we will summarise machine learning approaches for learning Ricci-flat metrics. For a more detailed discussion, we refer the reader to Ek et al. [3, Sections 2 and 3]. In Section 3 we motivate our main results by showing that symmetry group size is related to salience in learnt NN approximations, and discuss how various symmetries of Calabi–Yau metrics can be incorporated into ML models with Geometric Deep Learning formalism of Bronstein et al. [20]. In Section 3.3 we state our main theoretical results, namely a phenomenon that we call the *extrinsic symmetries* of Calabi–Yau manifolds, whereby both the Kähler potential of the flat metric and its related differential forms exhibit representations with strictly more symmetries than the manifold itself.* In Section 4 we experimentally validate our hypothesis on multiple families of Calabi–Yaus, achieve state-of-the-art loss on the Fermat Quintic, and do so much faster than previous approaches. Subsequently, we focus on extracting symbolic expressions for corrections to the Kähler potential from the machine derived models. In Section 5 we describe closed-form symbolic approximations that also exhibit low loss. We close off with Section 6.1 where we address the challenge of finding *exact formulae* for the Ricci-flat metric, and show that there exist non-trivial loci on the Calabi–Yaus where the flat metric is completely determined by its symmetries.

2 Background and Related Work

2.1 Machine Learning

Neural networks are *universal approximators*, meaning that in the limit of infinite size they can approximate any reasonably well-behaved function to an arbitrary degree of accuracy [21, 22]. For example, a two-layer MLP (Multi-Layer Perceptron) with non-polynomial activation is an universal approximator for any continuous, bounded function on a compact subset of \mathbb{R}^n [23]. On the other hand, a Graph Neural Network (GNN) such as GIN [24] is a universal approximator for similarly restricted functions that operate on graph inputs. There are a plethora of universal approximation guarantees for various other neural architectures. However, these guarantees may not reveal much about the *training process* itself or determining the optimal network parameters.

Due to their powerful approximating capabilities, neural networks can be used to solve regression tasks even when the ground truth is unknown in an explicit sense. When learning a function $f(x) = y$ using a dataset of (x, y) pairs, we can set up a loss function like $\mathcal{L} = |\hat{y} - y|$ or similar, where we use the caret ($\hat{\cdot}$) to distinguish a neural network approximation $\hat{f}(x) = \hat{y}$ from the true function. If y is unknown, but we know that f

*The name is thus a slight misnomer as “extrinsic” refers not to the manifold but to differential forms.

satisfies a condition $C(f(x)) = 0$, then we can adapt the loss to $\mathcal{L} = |C(\hat{y})|$. This is the guiding principle of physics inspired neural networks (PINNs) [25, 26].

PINNs approximately solve PDEs using a loss function that measures how well the neural network satisfies differential equations and initial conditions. Depending on the nature of the PDE and complexity of the underlying space, training can be a challenging exercise.

2.2 Calabi–Yau Manifolds

We define a Calabi–Yau manifold, or n -fold, to be a compact Kähler manifold of complex dimension n that has a nowhere vanishing holomorphic n -form. This form is known as the volume or top form and is denoted by Ω . Its existence implies that the first Chern class c_1 of the Calabi–Yau manifold vanishes. A seminal result by Yau [1] showed that these manifolds admit a unique metric with vanishing Ricci tensor in each of its Kähler classes.

Calabi–Yau manifolds are a cornerstone of superstring theory. In the 1980s, it was realised that these geometries play an important role in compactifying a higher dimensional theory of quantum gravity to reveal details of the four-dimensional physical universe [27]. Although there are a number of challenges in recovering the details of our physical universe through string compactifications, understanding Calabi–Yau manifolds is a key step towards making increasingly accurate phenomenological predictions in heterotic string theory.

In some settings, broader features of the particle spectra depend only on the *topology* of the Calabi–Yau geometry. For example, number of generations of particles one recovers in the standard embedding is $|\chi|/2$, where χ is the Euler characteristic of the manifold — a topological feature. Therefore, only some compactification settings will result in three generations of matter particles that we observe in the Standard Model of particle physics. However, the choices are many, and while the exact number of Calabi–Yau (CY) manifolds is unknown, the number of compactification settings can be as large as 10^{500} [28]. On the other hand, many other features of the four-dimensional particle spectra such as masses of fermions or physical coupling constants require not just topological features, but also the Ricci-flat metric of the underlying Calabi–Yau geometry. Therefore, a better understanding of such metrics is essential for progress in this field.

There are many ways to obtain a Calabi–Yau manifold, and a hypersurface construction is one of the most straightforward. A *hypersurface* is a zero locus of any (homogeneous) polynomial Q in \mathbb{P}^n , but it is Calabi–Yau only if $\deg Q = n + 1$, with dimension $d = n - 1$. This can be further generalised into complete intersection Calabi–Yaus (CICYs). Complete intersection varieties are a joint zero locus of multiple polynomials in an ambient space made of multiple projective spaces. The Calabi–Yau condition for complete intersections is $\sum \deg_i = \sum (n_i + 1)$, where \deg_i are the degrees of the polynomials, and the ambient space is $\mathbb{P}^{n_1} \times \mathbb{P}^{n_2} \times \dots \times \mathbb{P}^{n_k}$ [29, 30]. One can easily see that the Calabi–Yau condition for hypersurfaces is a special case of that for CICYs.

In this paper we focus exclusively on Calabi–Yau hypersurfaces, but we expect that our methods can be extended to CICYs as well. Specifically, we focus on the Fermat family of

Calabi–Yaus, defined as the zero locus of the following polynomial

$$Q_n: 1 + z_1^{n+1} + z_2^{n+1} + \dots + z_n^{n+1} = 0 \quad (2.1)$$

or, in homogeneous coordinates

$$Q_n: Z_0^{n+1} + Z_1^{n+1} + \dots + Z_n^{n+1} = 0 \quad (2.2)$$

In ambient spaces \mathbb{P}^n for $n = 2, 3, 4$, we define the Complex Torus, K3 manifold, and the Fermat Quintic as

$$Q_{\text{Torus}}: 1 + z_1^3 + z_2^3 = 0 \quad (2.3a)$$

$$Q_{\text{K3}}: 1 + z_1^4 + z_2^4 + z_3^4 = 0 \quad (2.3b)$$

$$Q_{\text{Quintic}}: 1 + z_1^5 + z_2^5 + z_3^5 + z_4^5 = 0 \quad (2.3c)$$

which have dimension $d = 1, 2, 3$, respectively. One can keep increasing the dimension, obtaining a Sextic 4-fold, and so on, and the relation $n = d + 1$ always gets preserved. The simplicity and symmetry of these polynomials has made Fermat d -folds a good benchmark for experiments [3, 19, 31, 32, 33, 34, 35, 36, 37, 38, 39, 40, 41, 42, 43], even though phenomenologically they might not be an exact match for the observable universe.

2.3 Machine Learning Ricci-flat Metrics

On a Calabi–Yau one can define a *metric* g , a matrix-valued function that satisfies conditions such as Kählerity ($\partial_k g_{ij} = \partial_i g_{kj}$) and positivity ($g > 0$). To be exact, a Kähler metric also needs to be positive, which is a subtle but important point. Such metrics are easily found. One can recall the Fubini-Study metric $g_{\text{FS}} = I/\|Z\|^2 - Z^\dagger \otimes Z/\|Z\|^4$ on a projective space. Then, its pullback $\iota^* g_{\text{FS}}$ is a Kähler metric on the Calabi–Yau.

We are motivated by physics to add another condition to the metric, Ricci-flatness, and obtain a metric that has vanishing curvature. This condition simplifies to $\partial\bar{\partial} \log \det g = \mathbf{0}_d$ for Kähler metrics. It is known from theory that the Ricci-flat metrics are rare among the Kähler metrics. In the case of Fermat Calabi–Yaus, the flat metric is unique up to a constant scaling factor.

Unfortunately, the original existence proof by Yau is non-constructive [1]. For decades, the only class of manifolds where the flat metric was known were toric varieties. There the problem is almost trivial and solutions date to the 19th century [44]. After over a century, Kachru et al. [45] produced a flat metric on a non-toric Calabi–Yau for the first time. They gave not a closed-form expression but a perturbative method, and they only computed the metric to the leading order in FI parameter ξ , but they argued that computing higher orders is also possible and requires solving systems of linear equations only. Beyond tori and K3, no known methods to find the flat metric exist yet.

Fortunately, we can find good enough approximations by optimizing neural networks with gradient descent. However, to make this approach viable, several theoretical results are needed. Firstly, the flat metric g_b and the pullbacked Fubini-Study metric $\iota^* g_{\text{FS}}$ are in the same cohomology class on Calabi–Yau, meaning that we can write

$$g_b = \iota^* (g_{\text{FS}} + \partial\bar{\partial}\phi) \quad (2.4)$$

where $\phi : \mathbb{P}^n \rightarrow \mathbb{R}$ is unique up to factors that vanish after $\iota^* \partial \bar{\partial}$, and ι^* is the pullback via Jacobians from homogeneous to local coordinates. Since ϕ is scalar-valued, optimizing it is much easier than g . This approach, named PhiModel by Larfors et al. [33], is the current standard to learn g_b . Its another advantage is that it enforces the partial derivative constraint for Kählerity on the neural network output by construction. A spectral network by Berglund et al. [35] forces ϕ to be homogeneous by carefully adapting the neural architecture. We will revisit spectral models in the next section.

Second modification to make ML viable is simplifying the loss function. A metric is Ricci-flat if the scalar curvature vanishes, and a naïve approach would be to define the loss function \mathcal{L}_{Ric} to be its absolute value. However, that would require taking fourth-order mixed derivatives of ϕ , which makes it hard to backpropagate through.

Instead, a surrogate loss is employed. From theory, the flat metric satisfies the Monge–Ampère equation:

$$\det g_b = \kappa \Omega \bar{\Omega} \quad (2.5)$$

where Ω is the volume form, and κ is a real constant. Furthermore, Ω is easily computable using the defining polynomial, and κ can be numerically approximated by integrating Eq. (2.5) over the Calabi–Yau. Crucially, the implication is bidirectional: a Kähler metric satisfying the Monge–Ampère equation is Ricci-flat, so we replace the Ricci loss \mathcal{L}_{Ric} with the σ -measure

$$\mathcal{L}_\sigma = \left| 1 - \frac{\det \hat{g}}{\det g_b} \right| = \left| 1 - \frac{\det \hat{g}}{\kappa \Omega \bar{\Omega}} \right| \quad (2.6)$$

Thus, the problem becomes finding ϕ that minimises \mathcal{L}_σ . This setup is similar to PINNs, which is to be expected since the fundamental problem of solving a PDE is shared between PINNs and this model. But, there are also notable differences, such as lack of initial conditions for the Ricci-flat metric, presence of additional structure and symmetries originating from the manifolds, and use of surrogate losses.

Using neural networks to approximate flat metrics, while well established by [19, 33, 34, 35, 36, 46] and others, nevertheless has several issues that are identified by Ek et al. [3]. Firstly, the metric g is also required to be positive definite, which is not directly enforced by generic neural networks. This would require the correction ϕ in the PhiModel to be *pluri-subharmonic* [35], but there are no known ways to guarantee this. Instead, the networks are biased to positive definiteness through careful initialisation: $g_{FS} > 0$, so if we set $\phi_{init} \approx 0$, and if the NN stays near its initialisation during training, then positive definiteness is likely conserved. However, there are no theoretical guarantees that this will happen in practice, and checking positivity *post-hoc* is difficult since the metric can violate positivity on a set of measure zero. This is unsettling because much of the theoretical apparatus relies precisely on positivity assumptions.

The second issue is that the σ -measure is not a perfect surrogate for Ricci loss. Having \mathcal{L}_σ be identically zero does imply that the metric is Ricci-flat, but there are no known convergence guarantees that minimizing one also reduces the other in the approximate case. In practice, there are instances of Calabi–Yaus with pathological metrics that have low \mathcal{L}_σ but diverging curvature, as can be seen in e.g. Hendi et al. [34] with their discontinuous approximations.

Despite these issues, neural networks are converging to low σ -loss orders of magnitude faster compared to other, more principled approaches such as the Donaldson’s algorithm [2] and its variants, and so they remain important when studying numerical flat metrics.

2.4 Explainable AI

Neural networks for all intents and purposes behave as black boxes, and their enormous parameter space makes it difficult to interpret how they produce their outputs. Explainable AI is a research area that tries to make NNs interpretable either by constructing interpretable architectures, or with *post-hoc* techniques that can be applied to already trained models. In order to construct a model that is interpretable by design, it is useful to take knowledge of symmetries into account.

Alternatively, one can completely abandon neural networks in favor of different, more explainable architectures. For example, Kolmogorov–Arnold Networks by Liu et al. [47] replace linear weights and non-linear activation functions with learnable splines, with the effect that very small KANs can match the performance of MLPs with orders of magnitude more parameters. They also have universality guarantees from the Kolmogorov–Arnold representation theorem [48, 49] similar to that of MLPs.

Yet another way to obtain interpretable formulae by construction is via symbolic regression. The best symbolic regression framework known to authors is PySR [50, 51], which implements a genetic algorithm in Julia backend that searches for a symbolic function by combining supplied primitives such as addition, multiplication, exponentiation, etc.

Meanwhile, the *post-hoc* methods generally use some gradient information to give each feature an attribution score measuring its effect on the loss. Such attribution score, or *saliency*, in its simplest form is

$$a_i = \frac{1}{n} \sum_{k=1}^n \left| \frac{\partial \mathcal{L}_\sigma^{(k)}}{\partial x_i^{(k)}} \right| \quad (2.7)$$

where i ranges over the features x , and k over entries in the dataset.

There are many different ways to assign attribution scores to neural network inputs. One popular method is integrated gradients by Sundararajan et al. [52]. However, methods like this are more suited towards “real-world data”. Integrated gradients in particular require computation with respect to a chosen baseline. This works fine with e.g. images, where the authors recommend taking a black image or white noise as baseline, but it becomes less clear how to translate this to the synthetic dataset of Calabi–Yaus. Here inputs are in \mathbb{P}^n , which does not have a mathematically distinguished origin point, so any choice of baseline would have to break the symmetry of the manifold in some way. Furthermore, PhiModel optimises for higher-order derivatives, so we can expect that simple gradient analysis already carries sufficient information about how inputs are used. And, since we use small models in our experiments, we do not suffer from vanishing gradients that might affect our attribution scores. Thus, the issues that necessitated creation of advanced methods like integrated gradients or LRP [53] are likely not applicable in this case. In fact, this simple gradient attribution of Eq. (2.7) has already led to new discoveries in knot and representation theory in Davies et al. [54].

3 Symmetric Forms on Calabi–Yaus

Calabi–Yau manifolds and their metrics are often highly symmetric, and a neural network that captures these symmetries will train more easily and achieve lower loss. Specifically, in this paper we look at Fermat Calabi–Yaus which have the following symmetries:

- \mathbb{C}^* projective symmetry inherited from embedding into a \mathbb{P}^n ambient space,
- \mathbb{Z}_2 conjugation symmetry as Q is invariant under conjugation,
- \mathbb{S}_n permutation symmetry as Q is symmetric,
- \mathbb{Z}_{n+1}^n toric symmetry as Q is invariant under actions $Z_j \mapsto e^{\frac{2i\pi}{n+1}k_j} Z_j$, for $k_j \in \mathbb{Z}_{n+1}$.

Berglund et al. [35] designed “spectral networks” that take matrix $A_{ij} = \left(\frac{Z_i \bar{Z}_j}{\|Z\|^2} \right)$ as input. Owing to well known results in invariant theory [55, 56], this network is invariant under the \mathbb{C}^* projective symmetry by construction, while also being able to approximate any \mathbb{C}^* -symmetric function in the infinite limit.

In Hendi et al. [34] more symmetries were added by arbitrarily defining one group element as fundamental, and mapping points on the CY to corresponding fundamental domains. This may create discontinuities at domain boundaries, and such networks may only be reducing σ -measure and not the underlying Ricci loss, but this may become addressed in the future by tweaking the architecture.

We take a different approach and give a blueprint for how these symmetries can be treated *naturally*, and in the spirit of Geometric Deep Learning of Bronstein et al. [20]. As mentioned above, the scaling symmetry is handled by using spectral networks. To capture invariance under toric symmetries it is sufficient to substitute coordinates Z with invariant features Z^n , which immediately follows from the following statement.

Proposition 3.1. *Let $\zeta^n = 1$ and $f : \mathbb{C} \rightarrow \mathbb{C}$ be a function with a rotation symmetry $f(z) = f(\zeta z)$. Then there exists $g : \mathbb{C} \rightarrow \mathbb{C}$ satisfying $f(z) = g(z^n)$.*

Proof. Let $\pi : z \mapsto |z|^{1/n} e^{i/n \arg z}$ be the principal n -th root. It satisfies $\pi(z^n) = z \zeta^k$ for some $k \in \mathbb{Z}$ as a function of z . Then, just take $g = f \circ \pi$, which is well defined and single-valued, and trivially satisfies $g(z^n) = f(\pi(z^n)) = f(z \zeta^k) = f(z)$. \square

Crucially, unlike the construction based on fundamental domains, the domain of g is the entire complex plane with no boundaries nor extra continuity conditions. To capture conjugation invariance, we can similarly replace (\Re, \Im) maps in the spectral network either with $(|\cdot|, \Re)$ or with $(\Re, |\Im|)$, both of which respect conjugation symmetry. Thus, we are only left with permutation symmetry to handle.

3.1 Permutation Symmetry of Calabi–Yaus

To encode permutation symmetries of Calabi–Yau coordinates we establish a connection between coordinates and graphs, which allows us to use GNNs instead of MLPs. For example, we can represent the permutation symmetries of K3 (Fig. 1) or Tian-Yau (Fig. 2)

with appropriately chosen graphs. Better still, a suitable graph can be constructed for any symmetry group [57].

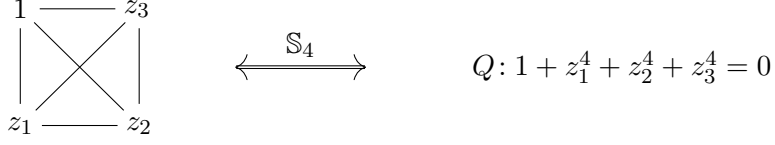


Figure 1. The symmetry group of a K3 defining polynomial (right), \mathbb{S}_4 , is also the automorphism group of the complete graph (left).

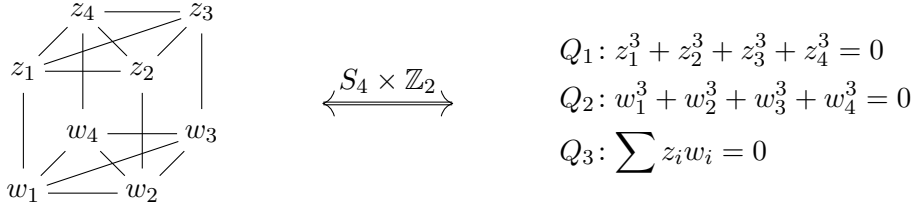


Figure 2. The symmetry of a Tian-Yau manifold (right), and a matching graph (left).

Thus, a complete pipeline that incorporates all of these symmetries can look like Fig. 3. We obtain good results when training neural networks this way, and report the σ -measures in Table 1. In contrast to Hendi et al. [34], we reduce Ricci measure as well.

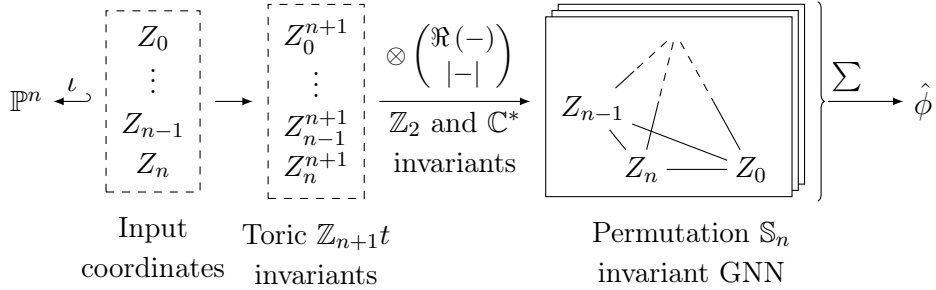


Figure 3. A complete pipeline that incorporates \mathbb{C}^* , \mathbb{Z}_2 , \mathbb{S}_n , and \mathbb{Z}_{n+1}^n symmetries into a NN model. Note that spectral features $Z_i \overline{Z_j}$ must be encoded into edge features of GNN layers in order to align with the permutation symmetries.

Despite these benefits, we do not pursue this approach further for several reasons, and we defer refinements and investigations using GNNs to the future. The first reason is that finding optimal invariants is very hard in general, although much progress has been made for free group actions [8]. The second reason is that we will conjecture that Fermat Calabi–Yaus have much larger symmetries inherited from the embedding in \mathbb{P}^n . This stands to significantly speed up machine learning approaches in highly symmetric situations. In contrast, the neural network and GNN approaches are more useful in less symmetric contexts, such as the Dwork family, where we do not find additional symmetries.

3.2 Saliency of Symmetric Features

To estimate the impact of different features on the loss, we train a model that uses many features with different symmetry groups. We use spectral features of Berglund et al. [35], as well as other more symmetric (0,0)-forms, and then compare their saliencies a_i defined in Eq. (2.7). The most symmetric expressions we look at are the power sum *symmetric polynomials*

$$s_k = \frac{\sum_i |Z_i|^{2k}}{(\sum_i |Z_i|^2)^k} \quad (3.1)$$

which we normalise to ensure they are degree 0 homogeneous. These are real polynomials, so they do *not* form a basis for symmetric functions of type $\mathbb{P}^n \rightarrow \mathbb{R}$. But, they *do* form a basis on $\mathbb{R}\mathbb{P}^n$, where we only need to use s_2, \dots, s_{n+1} because we always have $s_0 = n$ and $s_1 = 1$.

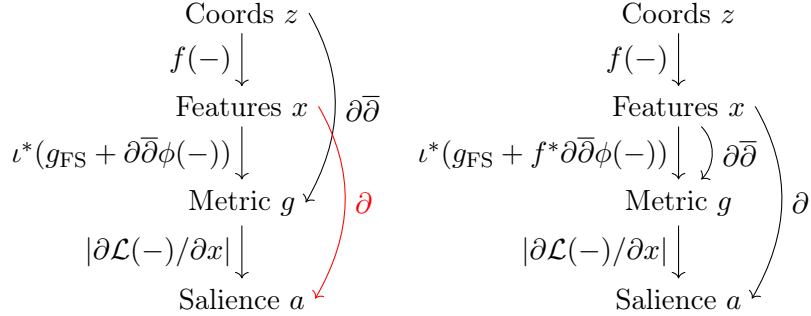


Figure 4. Computation graph of attribution weights, with arrows denoting dependencies. Left: differentiation with respect to features is impossible as it overlaps with an earlier one. Right: correct implementation with both differentiations in feature space.

The saliencies a_i cannot be computed in the PhiModel, as g and \mathcal{L}_σ are obtained by differentiating with respect to coordinates Z_i , while features $x = f(z, \bar{z})$ are in the middle of the computation graph and so are unavailable for differentiation. In order to compute them, we modify the PhiModel of Eq. (2.4) and replace differentiation $\partial\phi/\partial z$ in ambient space with differentiation $\partial\phi/\partial x$ in feature space via the chain rule in Appendix E. This approach is visualised in Fig. 4, and the resulting ansatz for the metric becomes

$$g = \iota^* \left(g_{\text{FS}} + \frac{\partial\phi}{\partial x_k} \frac{\partial^2 x_k}{\partial z_i \partial \bar{z}_j} + \frac{\partial^2 \phi}{\partial x_k \partial x_l} \frac{\partial x_k}{\partial z_i} \frac{\partial x_l}{\partial \bar{z}_j} \right) \quad (3.2)$$

where $\phi : \mathbb{R}^m \rightarrow \mathbb{R}$ is now a function of real features $x(z, \bar{z})$, and $x : \mathbb{P}^n \rightarrow \mathbb{R}^m$. Unlike Eq. (2.4), this expression *can* be differentiated with respect to x , because we can treat $\partial x/\partial z$ terms as constants, and only differentiate the $\partial\phi/\partial x$ terms. This also means that we can theoretically improve backpropagation, by precomputing the pullback to features and differentiating only up to x . We do not implement this optimisation, as the training loop is already sufficiently fast for our purposes.

In our experiment we use the same architecture and parameters as described in Section 4, with added weight decay of 5×10^{-4} to slightly optimise towards feature sparsity. We use

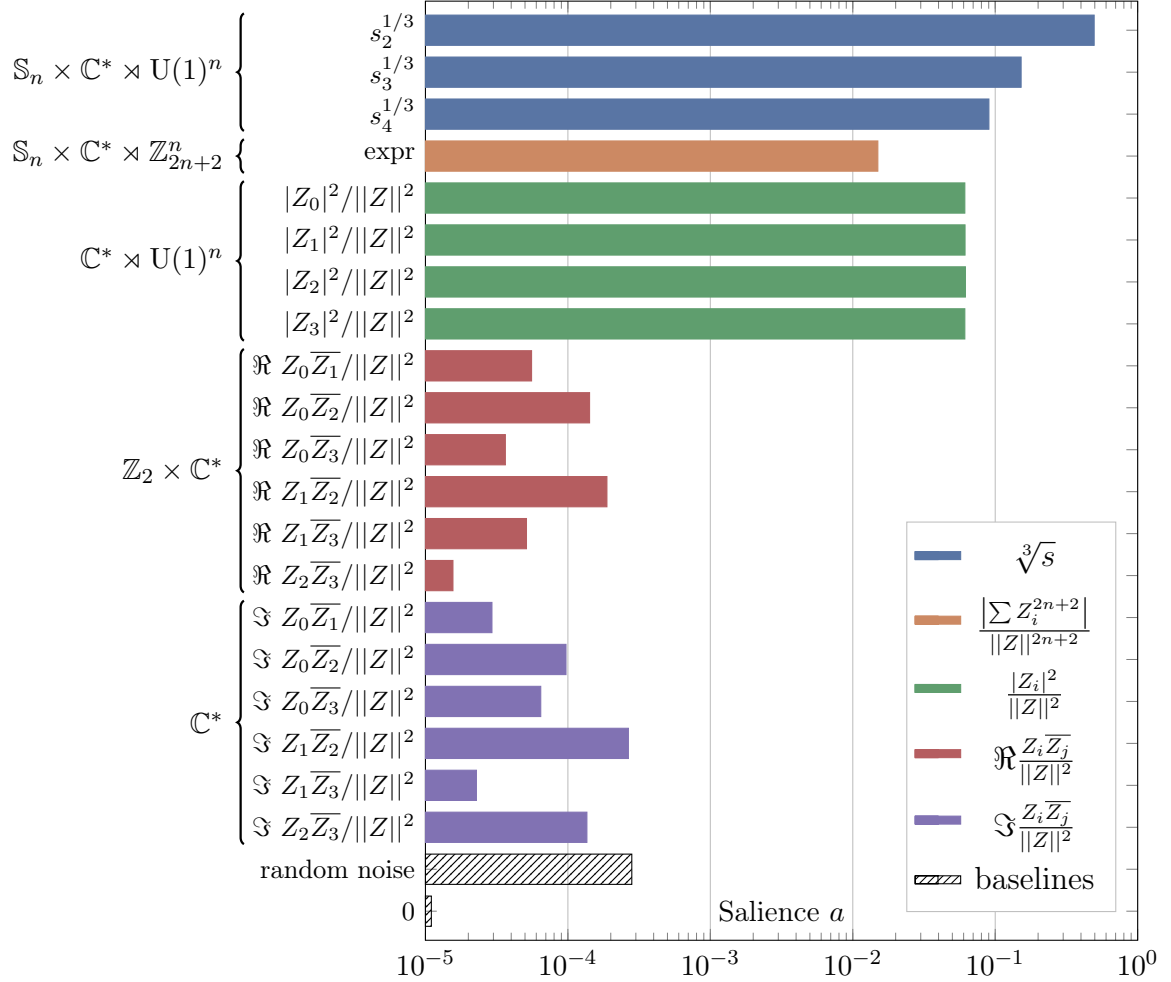


Figure 5. Relative salience a on K3 (log scale) on the test set. Larger score means higher attribution relative to other features so that total salience sums to 1. Here \mathbb{C}^* represents projective scaling symmetry, \mathbb{Z}_2 is conjugation invariance, \mathbb{S}_n is the permutation group, \mathbb{Z}_{n+1}^n is toric symmetry ($Z_j \mapsto e^{\frac{2i\pi}{n+1}k_j} Z_j$), and $\text{U}(1)^n$ is phase invariance ($Z_j \mapsto e^{i\phi_j} Z_j$).

random noise and 0 as baselines. Due to stochasticity, even the salience of a constant zero feature will never be zero — we observe that it is just above 10^{-5} . Notably, a constant non-zero feature would not be a valid baseline, as it would have much larger salience due to being equivalent to a bias term in the neural network.

We plot the distributions of a in Fig. 5 for the K3 manifold, scale them so that total salience is 1, and observe that:

- $\text{U}(1)$ symmetric features have higher salience, with **symmetric polynomials** s_k having by far the highest effect on the loss,
- **diagonal spectral features** $|Z_i|^2/\|Z\|^2$ have equal attribution, suggesting the network learnt permutation symmetry of the coordinates,

- salience of **off-diagonal spectral features** is two orders of magnitude below the next lowest feature, and on the same level as random noise.

For a similar analysis of features on a Fermat 3-fold, see Appendix D.

One may ask if this can be explained by larger symmetry groups having more influence on the metric. However, this will not do for several reasons. Firstly, size of the symmetry group is not directly correlated with salience. Secondly, off-diagonal elements are not just less salient than the more symmetric features. Rather, they are used as much as the uniform random noise, which is to say not at all. Thirdly, $U(1)^n$ is not a symmetry of the Calabi–Yau and does not preserve the defining polynomial, unlike its discrete subgroups — toric and conjugation symmetries $\mathbb{Z}_{n+1}^n, \mathbb{Z}_2 < U(1)^n$. However, features with $U(1)^n$ symmetry achieve a higher score nonetheless.

This raises the question of why symmetric polynomials s_k perform so well on Fermat Calabi–Yaus, despite having “incorrect” symmetries.

3.3 Extrinsic Symmetries of Calabi–Yau Hypersurfaces

To answer this, and to state the main theoretical results of our paper, we will need to consider three important scalar forms.

The first is the defining polynomial for the Calabi–Yau Q , with coordinates from the ambient space \mathbb{P}^n . The second and third, respectively, are the correction term ϕ and the integration weights $w = d\text{Vol}_\Omega/d\text{Vol}_{\text{FS}} = \det g_b/\det \iota^*g_{\text{FS}}$, whose domain is the Calabi–Yau.

We wish to make a statement about their symmetry groups Sym under which they are invariant, i.e. groups where $g \in \text{Sym}(f)$ iff $f(x) = f(g.x)$. Focusing on these quantities might seem artificial at first, but ϕ and w are already connected because both quantify the difference between g_b and ι^*g_{FS} . It can be argued that

$$\text{Sym}(\phi) = \text{Sym}(w) = \text{Sym}(Q) = \text{Isom}(\text{CY}, g_b)$$

where $\text{Isom}(\text{CY}, g_b)$ is the group of isometries (distance-preserving maps) of the metric on the manifold. It seems there is nothing else left to say, but there is.

Conjecture 3.2 (Extrinsic Symmetries). *Suppose $w^\mathbb{P}$ is an extension of w to the ambient space \mathbb{P}^n , such that $w^\mathbb{P}|_{\text{CY}} = w$ and $\text{Sym}(w^\mathbb{P}) \geq \text{Sym}(Q)$. Then, there exists a similar highly symmetric extension $\phi^\mathbb{P}$ such that*

$$\text{Sym}(\phi^\mathbb{P}) = \text{Sym}(w^\mathbb{P}) \geq \text{Sym}(Q) = \text{Isom}(\text{CY}, g_b)$$

Observe that w is known while ϕ is not. Thus, the conjecture says that if we can produce a good lift $w^\mathbb{P}$, then we can exploit the larger symmetry group when learning ϕ . This leads us to consider suitable choices for the lift $w^\mathbb{P}$.

Theorem 3.3 (Integration Weights Identity). *On any Calabi–Yau hypersurface embedded into \mathbb{P}^n with a defining polynomial Q , the integration weights $w = d\text{Vol}_\Omega/d\text{Vol}_{\text{FS}}$ satisfy*

$$w = \frac{\|Z\|^{2n}}{\|\nabla Q\|^2}$$

where $\|\cdot\|$ is the quadratic norm of vectors of coordinates Z and gradients ∇Q .

Proof. See Appendix A. □

We propose to take precisely the formula for w from Theorem 3.3, which is already well defined on the entire \mathbb{P}^n , and apply Conjecture 3.2 to it in order to get a large symmetry group, which does not need to be constrained either by $\text{Isom}(CY) = \text{Sym}(Q)$, or even by $\text{Isom}(\mathbb{P}^n) = \text{PU}(n)$. In the next section we will focus on families of Calabi–Yaus where this symmetry group is strictly larger than $\text{Isom}(CY)$, which will induce novel constraints on ϕ .

From Conjecture 3.2 and Theorem 3.3 we can deduce the following:

Proposition 3.4 (Existence of Individual $U(1)$ Symmetry). *Assume Conjecture 3.2. Then, if a variable Z_i only appears as a monomial Z_i^{n+1} in Q , then ϕ is invariant to changes in $\arg Z_i$ and depends only on $|Z_i|$.*

Proof. From Theorem 3.3 we compute that $w^{\mathbb{P}}$ depends only on $|Z_i|$. Depending only on $|Z_i|$ is equivalent to being $U(1)$ invariant with respect to this coordinate, so this property propagates to ϕ according to Conjecture 3.2. □

We note that the isometry group of the Calabi–Yau, $\text{Isom}(CY)$, is closely related to the Killing vector field, in that $\text{Isom}(CY)$ is continuous iff the Killing vector field exists [58, Proposition 18.9.]. Therefore, if the Killing vector field vanishes then the manifold has no continuous symmetries. This is the case for the 3-dimensional Calabi–Yaus, for example. Significantly, this is not in conflict with Proposition 3.4, because we are characterizing not $\text{Isom}(CY)$, but a potentially larger group $\text{Sym}(\phi^{\mathbb{P}})$.

In passing, we also note that Theorem 3.3 can be generalised to CICY manifolds embedded into \mathbb{P}^n with multiple defining polynomials Q_i . There, weights become $w = \|Z\|^{2n} / \prod \|Q_i\|^2$ and proof strategy is similar to that in Appendix A. However, we do not pursue this direction further as we do not focus on CICYs in this paper.

To end this section, we wish to emphasise that these statements should not be taken as a “final” theoretical explanation of this phenomenon. Rather, they are observations with great predictive power (Sections 4.1 and 4.2) that sometimes still fall short of capturing the full picture (Section 4.3).

4 Neural Network Approximations to ϕ

In this section we study performance of neural networks when learning ϕ from the perspective of our framework. We show that Proposition 3.4 has substantial experimental support, and that it can significantly simplify calculations in cases such as the Fermat family. We use the *cymyc* library by Berglund et al. [46] as it implements the training pipeline in JAX [59] and leverages JIT compilation, which we observe makes training much faster compared to alternatives written in TensorFlow. We use neural networks and not KANs or symbolic regression, because taking multiple symbolic derivatives in the training pipeline makes the latter impractically slow.

4.1 The Fermat Family

On Fermat Calabi–Yaus we can easily use Theorem 3.3 to compute $w = \|Z\|^{2n} / \sum |Z_i|^{2n}$. Then, using Proposition 3.4 (and assuming Conjecture 3.2) we immediately arrive at the following result:

Proposition 4.1. *Assume Conjecture 3.2. Then, for Fermat Calabi–Yaus defined by Eq. (2.1), the correction ϕ from Eq. (2.4) is a real function of absolute values of coordinates:*

$$\phi(z, \bar{z}) = f(|z_1|, |z_2|, \dots, |z_n|) \quad (4.1)$$

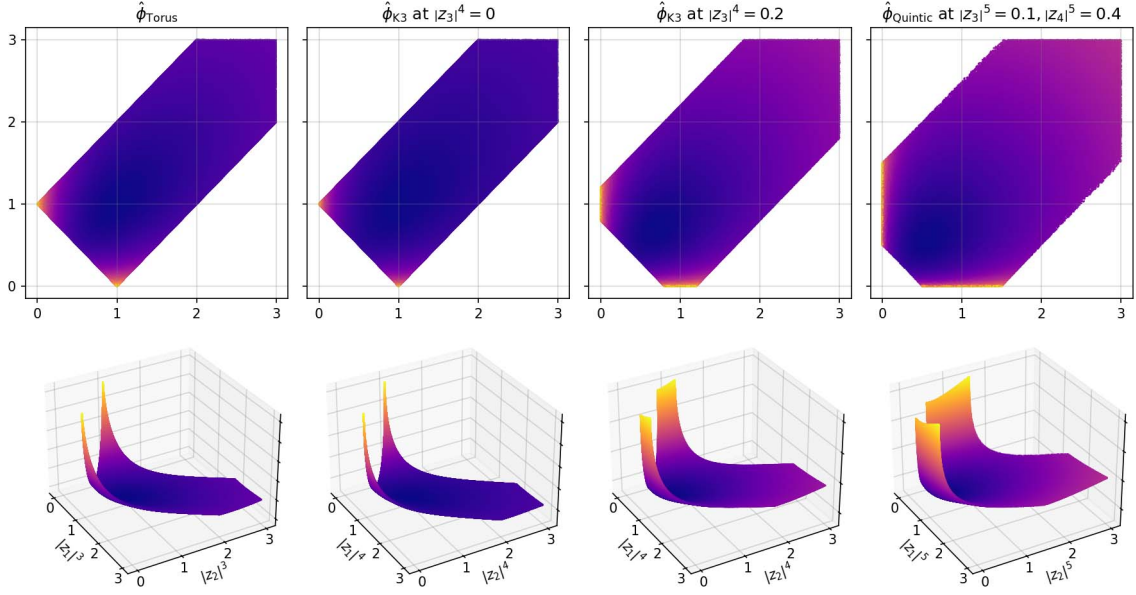


Figure 6. Leftmost: $\hat{\phi}_{\text{Torus}}$ versus $|z_1|^3$ and $|z_2|^3$. Middle: $\hat{\phi}_{\text{K3}}$ versus $|z_1|^4$ and $|z_2|^4$ for fixed $|z_3|$. Rightmost: $\hat{\phi}_{\text{Quintic}}$ versus $|z_1|^5$ and $|z_2|^5$ for fixed $|z_3|$ and $|z_4|$. Coordinates are plotted on x and y axes, while $\hat{\phi}$ is plotted on the z -axis and used to colour the figures. In all cases $\hat{\phi}$ behaves as a proper function of $|z_i|$: any choice of $|z_i|$ coordinates uniquely determines a point along the $\hat{\phi}$ axis, agreeing with Proposition 4.1. Also note the similarity between all figures, especially the two left ones.

Plots of ML approximated $\hat{\phi}$ versus the absolute values $|z_i|$ are shown in Fig. 6. We can prove this dependence directly in the one-dimensional case, without resorting to the theorems, because there *every* suitably symmetric function is dependent on absolute values only.

Proposition 4.2. *On the complex torus with the defining polynomial $Q = 1 + z_1^3 + z_2^3 = 0$, every $\mathbb{Z}_2 \times \mathbb{Z}_3^3$ -symmetric function f can be parameterised using only absolute values of coordinates.*

Proof. Firstly, by Proposition 3.1 f must admit parameterisation in terms of z_i^3 due to toric symmetries of Q and f , that is, due to invariance under rotation of z_i by the 3rd root of unity $\exp \frac{2i\pi}{3}$.

Secondly, $\Re z_i^3$ are expressible in terms of norms via $Q = 0$, for example:

$$\Re z_1^3 = \frac{1}{2} (|z_2|^6 - |z_1|^6 - 1)$$

Thirdly, $\Im z_i^3 = \pm \sqrt{|z_i|^6 - (\Re z_i^3)^2}$ are also functions of norms, up to a \pm sign, which is free and corresponds to the conjugation symmetry of Q and f .

Taking the above together, we obtain that f is a function of the norms $|z_i|$ as desired. \square

From this, Proposition 4.1 for the complex torus follows immediately without invoking Conjecture 3.2. However, this proof strategy fails in higher dimensions where we have functions that really do depend on the entire coordinates, not just their absolute values.

Proposition 4.3. *There exist highly symmetric functions on high-dimensional Calabi–Yaus which cannot be parameterised using the absolute values of coordinates only.*

Proof. We will construct an example on K3. Consider the locus given by $z_3 = e^{\frac{i\pi}{4}}$, where $z_1 = e^{i\phi}$, $z_2 = e^{i(\frac{\pi}{4} + \phi)}$. Firstly, we verify that it indeed lies on the Calabi Yau because $1 + \sum z_i^4 = 0$. Secondly, we consider the function $f(z, \bar{z}) = 1 + \sum z_i^8$. On the locus it simplifies to $2 + 2e^{8i\phi}$, which is not constant due to dependence on ϕ . But, we also have that $|z_1| = |z_2| = |z_3| = 1$ are all constants, which completes the proof. \square

Thus we see that Conjecture 3.2 and Theorem 3.3 allow us to make non-trivial statements about Fermat Calabi–Yaus, such as the Proposition 4.1.

4.1.1 Machine Learning ϕ with ModNet

To test Proposition 4.1 computationally, we train a neural network that learns ϕ only from coordinates’ absolute values. However, we obtain poor results with architectures like MLP ($|z_1|, \dots$). This is because the flat metric depends on the *derivatives* of ϕ . Here the only non-trivial derivatives arise from the activation function, which limits model expressivity. Instead, we will use the symmetric polynomials s_k defined in 3.1 reproduced below

$$s_k = \frac{\sum_i |Z_i|^{2k}}{(\sum_i |Z_i|^2)^k}$$

Our model, ModNet, becomes

$$\hat{\phi} = \text{MLP} \left(\sqrt[n+1]{s_k^j}, \text{ for } j, k \in \{1, \dots, n+1\} \right) \quad (4.2)$$

We use 2 layers of dimension 64 and GELU activation. Because inputs depend only on absolute values $|Z_i|$, so $\hat{\phi}$ too depends only on the absolute values. As the inputs are scale-invariant, $\hat{\phi}$ is a valid function on \mathbb{P}^n by construction.

With our ML pipeline that uses s_k we can improve upon previous approaches while being highly memory-efficient and training only for minutes on commercially available GPUs. We also perform much better than the GNN pipeline we proposed earlier. We train for 5 epochs with batch size of 4096 (largest possible on our hardware) on a dataset of 10^6 points.

Table 1. σ -measure for Fermat Calabi–Yaus. FS metric baseline is equivalent to setting $\phi = 0$. We omit [32, 38, 39, 60] as they do not evaluate the σ -measure.

Model	Fermat CY			
	Torus	K3	Quintic	Sextic
	Eq. (2.3a)	Eq. (2.3b)	Eq. (2.3c)	
Fubini-Study metric ($\iota^* g_{\text{FS}}$)	0.1015	0.2617	0.4985	0.5217
Jejjala et al. [19] [†]	—	0.068	0.18	—
Gerdes et al. [37] [‡]	—	—	0.05	—
Anderson et al. [43] [§]	—	—	0.05	—
Ashmore et al. [36]	—	—	0.021	—
Douglas et al. [31]	—	—	0.019	—
Ek et al. [3]	—	—	0.01	—
Larfors et al. [33]	—	—	0.0086	—
Berglund et al. [35] [¶]	—	4.2×10^{-4}	0.0030	—
Hendi et al. [34]	—	—	0.0027	—
GNN, Fig. 3	1.9×10^{-4}	8.8×10^{-4}	0.0119	—
ModNet, Eq. (4.2)	2.6×10^{-5}	3.7×10^{-4}	0.0010	0.0014
Distilled formula, Eq. (5.1)	3.6×10^{-5}	3.9×10^{-4}	0.0011	—
Compressed formula, Eq. (5.2)	4.4×10^{-5}	6.5×10^{-4}	0.0011	—

We use Adam with learning rate of 10^{-4} and exponential decay to 10^{-5} . We initialise weights with variance of 10^{-4} .

Our result for the Quintic corresponds to the Donaldson’s algorithm using global sections of degree $k = 52$, as per the scaling law by Douglas et al. [31]. We also perform tests on higher-dimensional CYs ($d > 4$), where our model behaves similarly. However, testing on larger dimensions exacerbates numerical issues, as the normalisation constant κ from Eq. (2.5) decays exponentially with dimension of Calabi–Yau.

As discussed in Section 2, one can have metrics with low σ -measure but high curvature, and for this reason it is important to check other properties of the trained model also, including the Ricci curvature R itself.

Table 2 shows that our model achieves the most accurate predictions for a variety of different topological quantities. In particular, while Hendi et al. [34] observed an increase in \mathcal{R} -measure when encoding symmetries with fundamental domains, our ModNet does not exhibit this pathological behaviour.

The middle column reports the largest value that real part of the 3rd Chern class c_3 achieves on the Calabi–Yau. The integral of c_3 is the Euler characteristic χ , and it equals -200 for the Quintic. Being a topological invariant, χ is always the same whichever metric

[†]Resulting metrics are not Kähler

[‡]Result inferred from Fig. 3

[§]Result inferred from Fig. 1

[¶]Result inferred from Fig. 31, and our own re-evaluation.

Table 2. Test measures on the Fermat Quintic Eq. (2.3c), estimated with MC integration on the manifold. Our ModNet achieves the best score with respect to every metric.

Model	Measure (test set)				
	σ -measure	\mathcal{R} -measure	$\max_{\text{CY}} c_3$	$\ R_{ij}\ $	$\ R_{ij} - \frac{1}{2}g_{ij}R\ $
FS metric (ι^*g_{FS})	0.4985	0.2278	561.63	0.3511	179.00
Flat metric (g_b)	0	0	unknown	0	0
Berglund et al. [35]	0.0030	0.0083	—	0.0161	12.2
Hendi et al. [34]	0.0027	0.0956	—	—	—
ModNet, Eq. (4.2)	0.0010	0.0028	1.90	0.0039	2.25
Compressed Eq. (5.2)	0.0011	0.0029	2.07	0.0045	0.93

one integrates. Berglund et al. [35] observe $\chi \approx -196.43$ in their integrations, but this discrepancy is purely numerical. We integrate over 5×10^6 points, which is 90x more, and produce $\chi \approx -199.3 \pm 0.1$ with either flat, Fubini–Study, or even random metrics. Again, this is expected because “Chern classes are independent of the choice of connection, but [...] different connections will lead to different representatives of the cohomology classes” [61], so $c_3(J_1) = c_3(J_2) + \partial\omega$ for any J_1, J_2 . Calabi–Yau is compact, so $\int \partial\omega = 0$, and we conclude that $\int c_3(J)$ is independent of the choice of complex structure J , which is to say that it is independent of the metric. On the other hand, $\max c_3$ is not a topological invariant, and it yields strikingly different values for Fubini–Study and flat metrics. The precise value of $\max c_3$ for the flat metric is unknown, but based in Table 2 we can conjecture that $c_3(J_b) \leq 0$, which could be a hint towards an unknown Bogomolov–Yau-type inequality [62, 63] for c_3 . The distribution of c_3 is shown in Fig. 7 (left). Finally, note the performance of our compressed model, which we will introduce shortly.

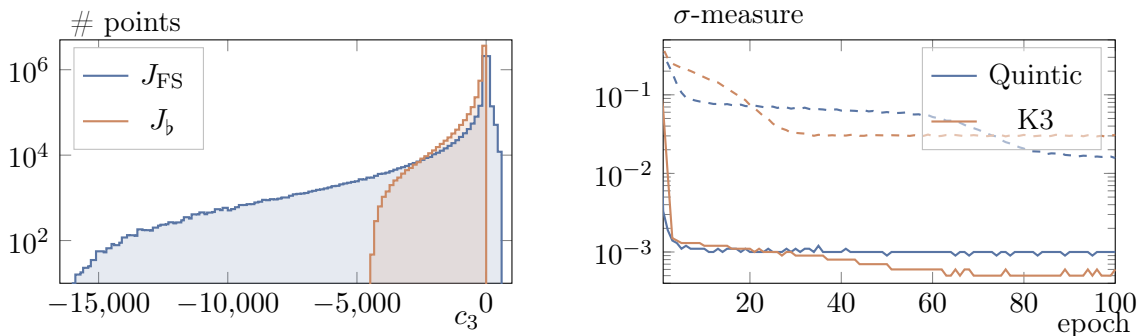


Figure 7. Left: Distribution of c_3 for flat and Fubini–Study metrics over 5×10^6 points on the Quintic. Right: Loss curves of ModNet (solid) vs Spectral Network (dashed) for K3 and Quintic.

In Fig. 7 (right) we plot loss curves in the small architecture regime (2 hidden layers of size 32). We see here that in our more symmetric context ModNet outperforms the spectral network, suggesting its performance should not be attributed to model architecture

but rather to the use of symmetric polynomials, which are better predictors than spectral features in the specialised case of the Fermat Calabi–Yaus.

Now that we looked at the Fermat family in great detail, we will quickly go over some other symmetric Calabi–Yaus.

4.2 The 0–1 Mixed Family

First, consider a family embedded into \mathbb{P}^n via

$$Q_n: Z_0^{n+1} + Z_1^{n+1} + \dots + Z_n^{n+1} - (n+1)\psi Z_0^n Z_1 = 0 \quad (4.3)$$

which we name the 0–1 mixed family. From Theorem 3.3 we compute that

Proposition 4.4. *The integration weights on the 0–1 mixed CY are*

$$w = \frac{(|Z_0|^2 + |Z_1|^2 + \dots + |Z_n|^2)^n}{|Z_0|^{2n-2} |n\psi Z_1 - Z_0|^2 + |\psi Z_0^n - Z_1^n|^2 + \sum_{k=2}^n |Z_k|^{2n}} \quad (4.4)$$

Observe that this defining polynomial depends only on absolute values of each coordinate except Z_0 and Z_1 . Therefore, Proposition 3.4 predicts that ϕ can be parameterised using these $n+3$ terms only:

$$\phi = f\left(\frac{|Z_0|^2}{\|Z\|^2}, \frac{|Z_1|^2}{\|Z\|^2}, \dots, \frac{|Z_n|^2}{\|Z\|^2}, \Re \frac{Z_0 \bar{Z}_1}{\|Z\|^2}, \Im \frac{Z_0 \bar{Z}_1}{\|Z\|^2}\right) \quad (4.5)$$

This is a theoretical prediction, and it is tentative as it requires assuming Conjecture 3.2. However, it is in excellent agreement with experimental results, just like the Fermat family. In Fig. 8 we indeed see that, just as we had predicted, only **diagonal elements** and **off-diagonal elements that mix Z_0 and Z_1** are salient. Meanwhile, salience of **other diagonal elements** is orders of magnitude smaller. In fact, it is consistent with salience of random noise, which we plot using a dashed black line. Thus, Fig. 8 supports our theoretical result that these features are likely not used in the flat metric.

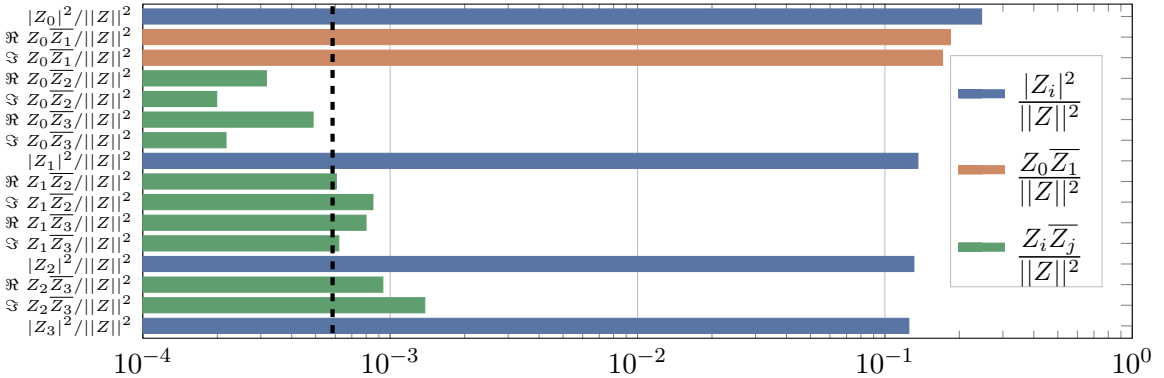


Figure 8. Salience of spectral features on a 2-dimensional 0–1 mixed CY ($n = 3, \psi = 2 + i$). Black dashed line is the baseline salience of uniform random noise.

Similarly, if we pick $\psi \in \mathbb{R}$ then we obtain conjugation symmetry, which eliminates dependency on $\Im Z_0 \overline{Z_1}$ according to Conjecture 3.2. Again, we observe this in practice in Fig. 9, where most features are used as much as random noise. In particular, the $\Im Z_0 \overline{Z_1}$ feature that was highly salient in Fig. 8 is almost completely unused here.

We have to draw attention to a subtlety regarding the conjugation symmetry. Namely, if $\psi \in \mathbb{R}$ then one can easily deduce that the defining polynomial Q is conjugation invariant, and from this conclude that ϕ should be invariant under the map $Z \mapsto \overline{Z}$. Then the discussion in Section 3 implies that one should use conjugation invariant features $|\Im Z_i \overline{Z_j}|$, and this indeed is the best possible feature to use assuming no other constraints are known. However, what we observe in Fig. 9 is not just that ϕ only depends on $|\Im Z_i \overline{Z_j}|$ instead of on $\Im Z_i \overline{Z_j}$, but that ϕ *does not depend on it at all*, a result that is only accessible through Conjecture 3.2.

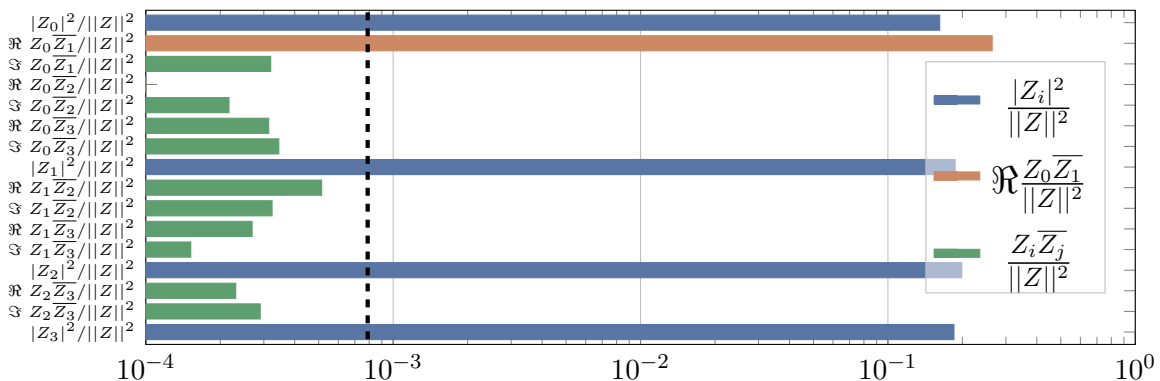


Figure 9. Saliency of spectral features on a 2-dimensional 0–1 mixed CY ($n = 3, \psi = 0.8$). Black dashed line is the baseline saliency of uniform random noise.

4.3 The Dwork Family

We also look at the Dwork family, defined via

$$Q_n: Z_0^{n+1} + Z_1^{n+1} + \cdots + Z_n^{n+1} - (n+1)\psi \prod Z_i = 0 \quad (4.6)$$

Note that we choose to scale the multiplicative term by $n+1$ for later convenience. This family is a non-example for our conjecture, because the integration weights w satisfy

$$w = \frac{(\sum |Z_i|^2)^n}{\sum_i |Z_i^n - \psi \prod_{j \neq i} Z_j|^2}$$

and here we fail to find symmetries that were not already present in Q_n . Thus we cannot immediately deduce which reduced set of features to use — Conjecture 3.2 is not applicable, so we would depend on $2n+2$ real and imaginary parts of coordinates. However, we empirically observe that we can train a neural network that matches spectral networks but uses only $n+1$ features: symmetric polynomials s_2 to s_{n+1} , and w . We take this to mean that deforming the Calabi–Yau with $\prod Z_i$ breaks symmetries in a way that requires

including one more parameter. Furthermore, we note that this does not trivially generalise: features s_2 to s_{n+1} and w are not enough to learn the flat metric on other highly symmetric Calabi–Yaus, such as the Cefalú quartics [35, 64] defined by

$$Q: Z_1^4 + Z_2^4 + Z_3^4 + Z_4^4 - \frac{\lambda}{3}(Z_1^2 + Z_2^2 + Z_3^2 + Z_4^2)^2 = 0$$

Thus this behaviour anticipates a finer handling of symmetries than what is done in this paper, and we hope that it will inspire future work. For now, we return to the Fermat Calabi–Yaus as we already understand them well enough, and there show that our symmetry arguments allow us to move from neural networks into the realm of closed form expressions.

5 Symbolic Approximations to ϕ

In this section, we demonstrate how the black-box NN approximations can be distilled into interpretable formulae, *with negligible impact to loss*. Specifically, we distill our approximations for ϕ on Fermat Calabi–Yaus into short expressions involving symmetric polynomials s_k .

We will often focus on 3-folds since they represent the extra dimensions in the 10-dimensional heterotic string theory. However, we are interested in the entire Fermat family, in order to show that it exhibits patterns in its flat metric which are generalisable across dimensions d .

We do not focus on the Kähler potential K in this section, because formulae for ϕ can always be converted into formulae for K as $K_b = K_{\text{FS}} + \phi$, but the other direction is nearly impossible due to an implicit change in coordinates. An example of this is Proposition 5.1. It gives a local Kähler potential for the flat metric on the torus, but a global formula for ϕ is still unknown and thus worth studying.

Proposition 5.1. *Consider a complex torus hypersurface, and the canonical coordinate chart with a local coordinate $x = Z_2/Z_1$, and Z_3 eliminated via $Q(Z_1, Z_2, Z_3) = 0$. Then, one possible Kähler potential of the flat metric can be obtained as*

$$K_b(x, \bar{x}) = \left| \int \Omega(x) dx \right|^2$$

On the torus given by $Q(Z_1, Z_2, Z_3) = Z_1^3 + Z_2^3 + Z_3^3 = 0$, we have $\Omega = e^{-\frac{2i\pi}{3}}(1+x^3)^{-\frac{2}{3}}$, so

$$K_b(x, \bar{x}) = \left| \text{Beta}\left(-x^3; \frac{1}{3}, \frac{1}{3}\right) \right|^2$$

where $\text{Beta}(x; a, b) = \int_0^x t^{a-1}(1-t)^{b-1} dt$ is the incomplete Beta function.

We begin our symbolic analysis by plotting the correlation between ϕ and s_2 for multiple Calabi–Yaus in Fig. 10. We observe that this correlation is strong, but also non-linear. For the torus in particular, ϕ is very close but still not exactly equal to a scalar multiple of s_2 . The nonlinearity for the torus is so small that it cannot be deduced from Fig. 10, nor with

standard statistical tools. In fact, for all Calabi–Yaus we find that the p -value associated with a linear regression is so small that it physically cannot be stored as a floating point number, while the Pearson’s correlation r is consistently close to 1. Thus, one needs to use different tools to explore these correlations. For example, on the torus one can find the expression of the metric obtained from $\phi = \text{const} \cdot s_2$ and show that it cannot be flat for any choice of const .

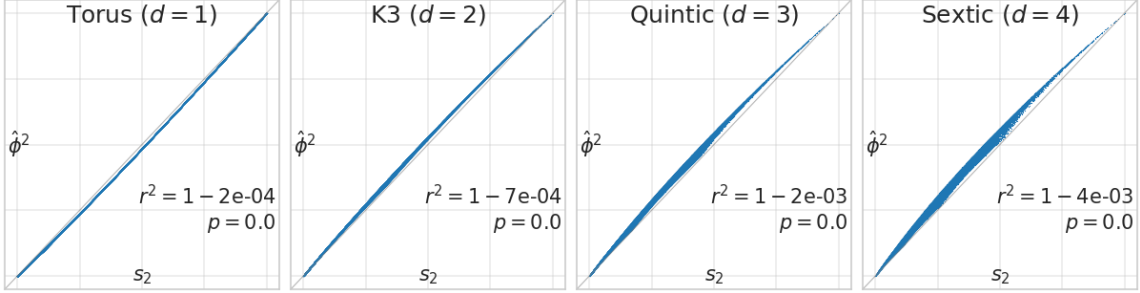


Figure 10. Correlation between s_2 (x -axis) and $\hat{\phi}^2$ (y -axis) for Fermat Calabi–Yaus. Axes have different scales. Important information is contained in the deviations from the straight line.

Our approach to studying $\hat{\phi}$ is to first distill the neural network into a symbolic form. We use the following ansatz, which we will motivate shortly:

$$\hat{\phi}_{\text{symb}} = \sum_i \sum_j c_{ij} \sqrt[n+1]{s_i^j} \quad (5.1)$$

We fit c_{ij} via least squares optimisation from our ML approximated $\hat{\phi}$, and report the exact values in Appendix B.

After distilling c_{ij} from ML oracle we validate that the resulting formula achieves low σ -loss on test set, and report this in Table 1. This validation step is important because a good approximation for ϕ does not have to approximate the metric g at all. A model example is a piecewise linear function that can fit ϕ to arbitrary precision, but whose derivative vanishes everywhere. Thus, to achieve a good fit for g , we need an ansatz with “interesting” derivatives, and we discovered empirically that taking the roots in Eq. (5.1) maintains low loss after distillation. Specifically, this construction works markedly better than a power series in s_k . In a later section we will further explore the importance of taking the roots of these expressions.

To see how much information we lose when distilling and how much room for improvement there is, we compute $|\hat{\phi}_{\text{ML}} - \hat{\phi}_{\text{symb}}|$ over the manifold and compare it to the machine epsilon for 32-bit floating point numbers.

Machine epsilon $\epsilon = 1.192 \times 10^{-7}$ is not the smallest positive number that can be represented with 32-bit floats under IEEE 754 [65] — that would be the subnormal 1.4×10^{-45} . Rather, ϵ is the smallest positive number that numerically satisfies $1 + \epsilon \neq 1$. The neural network is performing 32-bit computation, and its inputs are $O(1)$, so machine epsilon is a good bound on the resolution of $\hat{\phi}$, and Table 3 shows that we are reaching the theoretical limit with our models.

Table 3. Difference between $\hat{\phi}_{\text{ML}}$ and $\hat{\phi}_{\text{symb}}$ in units of machine epsilon ϵ .

Calabi–Yau	$\max_{\text{CY}} \hat{\phi}_{\text{ML}} - \hat{\phi}_{\text{symb}} $	
	Absolute	Relative to ϵ
K3	4.50×10^{-7}	3.8ϵ
Quintic	1.93×10^{-7}	1.6ϵ

5.1 Compressing Distilled Expressions

We also generate interpretable formulae by interacting with PySR package for symbolic regression [50, 51]. This way we discover a very compact approximation of the form

$$\hat{\phi}_{\text{symb}} = \text{poly}(s_i)^{\frac{1}{\pi}} \quad (5.2)$$

which we present in Table 4. Non-linear least-squares regression on polynomial coefficients converges in under a minute, and the end result has almost the same σ -loss as Eq. (5.1), but 3–5 times fewer parameters. For details behind this ansatz see Appendix C. In short, the exponent $\frac{1}{\pi}$ was determined empirically based on symbolic regression fits with PySR. This was performed on the torus, and then manually extended to higher dimensions. So, while it generalises well, it might not be locally optimal. This exponent could also be related to the same factor in the Fubini-Study potential, but due to lack of theoretical insight there is no obvious *a priori* reason why one would choose one exponent over another, or one formula over another.

Table 4. Compressed approximation for ϕ for different Fermat d -folds.

d	Symbolic $\hat{\phi}$	σ -measure	$\ R_{ij}\ $
1	$(0.00501 + 0.01102s_2 - 0.00157s_3)^{\frac{1}{\pi}}$	4.44×10^{-5}	0.00164
2	$(0.00022 + 0.0068s_2 + 0.00312s_3 - 0.0012s_4)^{\frac{1}{\pi}}$	6.46×10^{-4}	0.0053
3	$\frac{1}{5}(0.19s_2 + 1.83s_3 + 1.12s_2^2 - 1.5s_4 - 1.59s_2s_3 + 1.72s_5)^{\frac{1}{\pi}}$	0.0011	0.0045

We fit these coefficients with least squares against the neural network $\hat{\phi}$ prediction. But, this becomes harder because Eq. (5.2) is non-linear, and we cannot linearise it because ϕ is free up to a constant. These equations are also very sensitive to small changes in constants, which makes searching for them even more difficult.

Table 4 shows that a more informed choice of ansatz to distill into can yield formulae with even fewer parameters than Eq. (5.1). For example, for the Quintic we discover a formula with σ -loss that almost exactly matches the best neural network, but which only has *six* free parameters to fit versus ten thousand. This again points to existence of significant structure in ϕ . Approaches that are blind to this structure may therefore incur inefficiencies.

5.2 Towards the Root of the Problem

Earlier we motivated the use of n -th roots in Eq. (5.2) via their derivatives being “interesting”, but there is experimental motivation for this too. To see this, we first remark that ϕ (and

our approximation $\hat{\phi}$) can be interpreted as a purely real function $\phi : \mathbb{R}^n \rightarrow \mathbb{R}$ with inputs $x_i = |Z_i|^2 / \|Z\|^2$ according to Proposition 3.4 and Conjecture 3.2. Next, we study the correlation between $\hat{\phi}^{-1}$ and $\|\nabla\hat{\phi}\|_1$ and visualise it in Fig. 11.

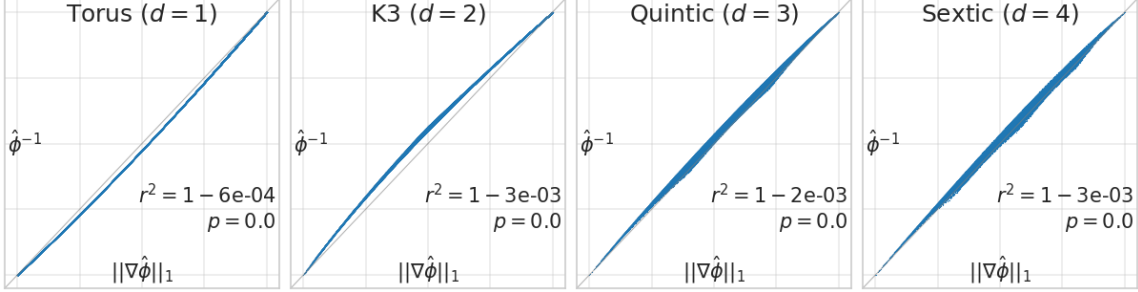


Figure 11. Correlation between $\hat{\phi}^{-1}$ and $\|\nabla\hat{\phi}\|_1$ for Fermat Calabi–Yaus of dimensions 1–4. Gradients are taken *with respect to features* $x_i = |Z_i|^2 / \|Z\|^2$. Axes have different scales.

From this, we can empirically derive that on Fermat Calabi–Yaus $\hat{\phi}^{-1} \sim \|\nabla\hat{\phi}\|_1$.

Proposition 5.2. For $\alpha \in \mathbb{R}^+$, $f : \mathbb{R}^+ \rightarrow \mathbb{R}^+$ the functional equation

$$\alpha f^{-n} = \|\nabla f\|_1$$

conditioned on $\sum x_i = 1$, where $\|\cdot\|_1$ is a L^1 -norm, is solved by

$$f = \left(\alpha \frac{n+1}{2} \sum x_i^2 \right)^{\frac{1}{n+1}}$$

Proof. One can compute $\frac{\partial}{\partial x_i} f = \alpha x_i f^{-n}$. Since the domain is \mathbb{R}^+ we have $\|\nabla f\|_1 = \sum \frac{\partial}{\partial x_i} f$. Using $\sum x_i = 1$ completes the proof. \square

A relationship between $\hat{\phi}^{-1}$ and $\|\nabla f\|_1$ from Fig. 11 thus produces an approximation $\phi \approx \sqrt{\alpha s_2}$, and is a possible underlying cause of the correlation between $\hat{\phi}^2$ and s_2 visible in Fig. 10. We say that the functional equation is “deeper” than this approximation, because the correlation between $\hat{\phi}$ and s_2 can be observed directly from Fig. 10, but in order to apply the functional equation from Proposition 5.2 and obtain Fig. 11, one first requires a specific parameterisation of $\hat{\phi}$ in terms of absolute values and this in turn requires our symmetry arguments and Conjecture 3.2.

Consider now what this means for ϕ . We found a PDE that it approximately satisfies, found a solution for it, and showed that it closely matches $\hat{\phi}$ itself back in Fig. 10. Now, ϕ is by definition a solution to a PDE, namely Monge–Ampère Eq. (2.5), which begs the question whether there exists a *different*, more solvable PDE that it also satisfies. Unfortunately, in the present case the formula $c\sqrt{s_2}$ is the worst performing distillate so far even though it approximates $\hat{\phi}$ well, but after slight modifications we arrive at Eq. (5.2) which has the best ratio of parameters to accuracy.

Fig. 12 shows that the over-parameterised regime of neural networks achieves the lowest loss, which is inversely proportional to the number of parameters. However, it also shows

that we can have both low loss and few parameters if we design custom ansätze that explicitly perform more complex calculations.

Note that a hypothetical closed-form expression for the flat metric would lie infinitely far on the bottom left of Fig. 12, because it would have no free parameters (for a fixed choice of complex structure moduli) and zero σ -measure because it is flat.

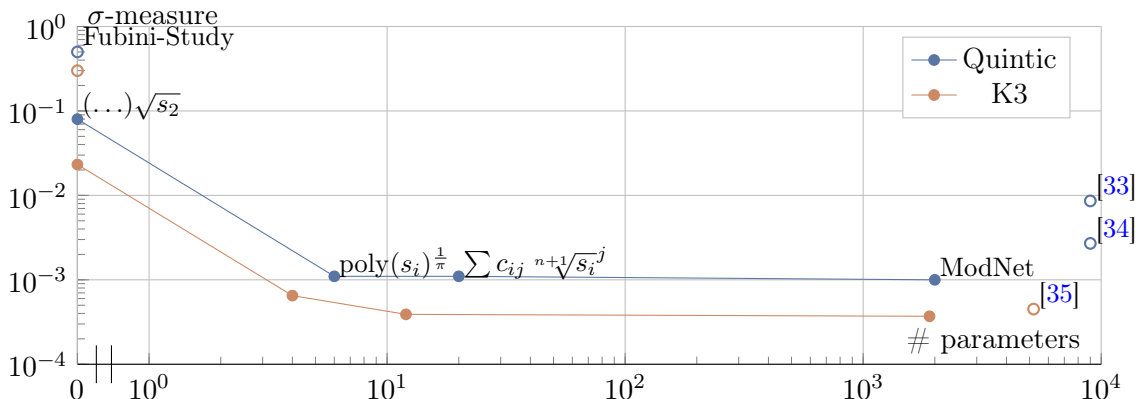


Figure 12. Pareto frontier of multiple symbolic approximations for ϕ , trading off number of parameters (x -axis) and σ -measure (y -axis). Filled points mark the frontier while empty points represent suboptimal results. Both axes are in log scale. Mind the discontinuity on the x -axis between 0 and 1. Near the top left “(...)” represents an expression with no parameters that is defined in Proposition 6.7, while constants in other formulae were fit numerically.

6 Analytical Properties of ϕ

So far we have shown how to use various symmetries of our learnt ML approximations to construct simple ansätze for nearly-flat metrics. This still does not explain how these relations arise in the first place, and whether they have any special meaning in the context of flat metrics. We concluded the last section by showing that one can find PDEs that yield good approximations to ϕ which could explain some of its behaviour. We are therefore motivated to investigate whether ϕ has other interesting analytical properties as well. In this section we thus turn to treating our approximations $\hat{\phi}$ more theoretically, as opposed to numerical experiments in previous sections. Firstly, we informally remark that our approximations $\hat{\phi}$ exhibit a curious pattern that is only visible *across multiple dimensions*:

Conjecture 6.1 (Informal). *On a d -dimensional Fermat Calabi–Yau, the correction ϕ is “related” to the correction one dimension up, with one coordinate zeroed out:*

$$\phi_d(Z_0, \dots) \sim \phi_{d+1}(0, W_1, \dots) \quad (6.1)$$

where Z is a point on the d -fold and W is a related point on the $d + 1$ -fold with $W_0 = 0$.

This “similarity across dimensions” can be seen in Fig. 6, where the plots are qualitatively identical despite originating from different Calabi–Yaus, suggesting that ϕ has a significant amount of structure.

We can partially explain this behaviour because $s_k(Z_0, \dots) = s_k(0, Z_0, \dots)$, but the exact relationship is unclear. We can also demonstrate this more directly.

Observe that we cannot directly compare the corrections ϕ of Calabi–Yaus with different dimensions, as they also have different defining polynomials and ambient spaces. However, if (Z_0, \dots, Z_{a+1}) is a point on Fermat Calabi–Yau of dimension a , then $(Z_0^{\frac{a}{b}}, \dots, Z_{a+1}^{\frac{a}{b}}, \underbrace{0, \dots, 0}_{b-a})$ is a point on Fermat Calabi–Yau of dimension $b > a$. Thus, this relation allows us to meaningfully link two different corrections on a subset of dimension a .

For example, take a Fermat 1-fold defined with $Z_0^3 + Z_1^3 + Z_2^3 = 0$, and a Fermat 2-fold defined with $W_0^4 + W_1^4 + W_2^4 + W_3^4 = 0$. Then, one can associate to each point (Z_0, Z_1, Z_2) on the 1-fold a point $(0, Z_0^{3/4}, Z_1^{3/4}, Z_2^{3/4})$, and it is easy to check that it indeed lies on the 2-fold. We claim that values of ϕ at these points are highly correlated, even though they come from different Calabi–Yaus.

As a side note, the association we present is not unique, because it involves taking a complex n -th root. Nevertheless, our claim is well-defined due to toric symmetries of ϕ , which make it invariant to the choice of the root branch.

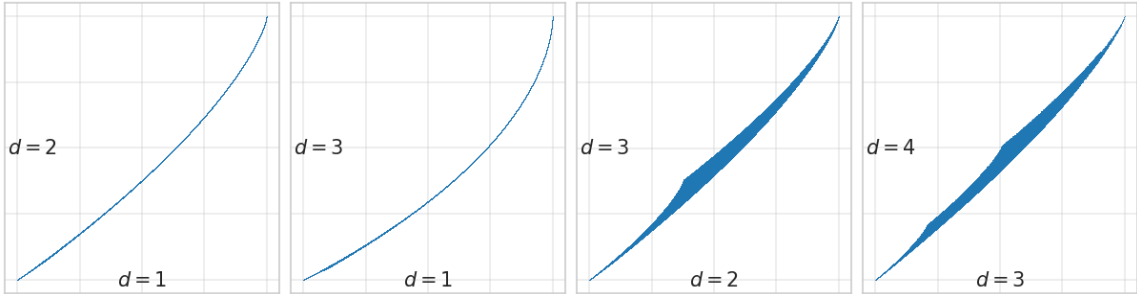


Figure 13. Correlation of $\hat{\phi}$ on different Fermat CYs. As explained above, smaller CYs’ coordinates are power-scaled to satisfy the defining polynomial of larger CYs, and extra coordinates are set to 0.

In Fig. 13 we plot such correlations for a range of different choices of dimensions. In each plot we again observe this “self-similarity” suggested by Conjecture 6.1. We also emphasise that both Figs. 10 and 11, and now also Fig. 13, share the same visual feature. Namely, scatter plots of $\hat{\phi}$ on CY of dimension d seem to have $d - 1$ sharp “corners” along it. It is surprising that this feature appears in all the plots, suggesting they may share a common explanation.

To make further statements about the analytic behaviour of ϕ , we first define some terminology. Assume a coordinate chart on the CY under the standard pullback, where $Z_0 = 1$ and local coordinates are $Z_1 \dots Z_n$. Then define the following loci on Fermat Calabi–Yaus.

Firstly, let the *pseudo-origin* be the origin in this local coordinate chart. This point is not uniquely defined in the ambient space, but our observations hold for each of them due to symmetries. In ambient space, the pseudo-origin has coordinates $(1, \sqrt[n+1]{-1}, 0, \dots, 0)$ up to permutation.

Next, the *equimodular locus* is the locus on Calabi–Yau defined by $|Z_0| = |Z_1| =$

$\dots = |Z_n|$. This submanifold has real dimension $d - 1$, where $d = n - 1$ is the complex dimension of the Calabi–Yau, because each of the n constraints reduces dimension by one. Our investigation predicts that ϕ will be constant on this submanifold, so we can expect to see interesting simplifications on it.

These loci are well defined and non-empty for all Fermat hypersurfaces. We also propose that they are interesting to study because on them the behaviour of ϕ and g_b can be conjectured or outright proven.

Conjecture 6.2. *The correction ϕ attains a global maximum at any pseudo-origin, and a global minimum on the equimodular locus. More generally, if we fix absolute values for some Z_i and vary the others, then the minimum is attained when the remaining coordinates have the same absolute value, and the maximum is attained when all but one of the free coordinates is zero.*

This conjecture says that ϕ is not just continuous and differentiable, but has sufficient analytic structure for stronger statements such as derivative bounds to be imposed on it.

Conjecture 6.3. *Consider a d -dimensional Fermat Calabi–Yau embedded into \mathbb{P}^n where $n = d + 1$. Then there exist constants $a, b, c \in \mathbb{R}$ with $0 < a < b, c$ such that the correction ϕ satisfies:*

$$\begin{aligned} -\frac{c}{|Z_i|^2} &< \frac{\partial_i \phi}{Z_i} < \frac{c}{|Z_i|^2} \\ -\frac{a}{|Z_i|^2} &< \partial_i \bar{\partial}_i \phi < \frac{b}{|Z_i|^2} \\ -\frac{b}{|Z_i|^2 |Z_j|^2} &< \frac{\partial_i \bar{\partial}_j \phi}{Z_i Z_j} < \frac{a}{|Z_i|^2 |Z_j|^2} \end{aligned}$$

Note that $\partial_i \phi / \bar{Z}_i, \partial_i \bar{\partial}_j \phi / \bar{Z}_i Z_j \in \mathbb{R}$ by Conjecture 3.2, so the inequalities are well-posed. In particular, we conjecture that the exponent 2 in the denominators is tight.

It follows from this conjecture that $\partial \bar{\partial} \phi$ decays as $1/|Z_i Z_j|$. Therefore, if we eliminate Z_n via pullbacks, then the deviation from the Fubini–Study metric given by

$$(\iota^* \partial \bar{\partial} \phi)_{ij} = \left(\partial_i - \frac{Z_i^n}{Z_n^n} \partial_n \right) \overline{\left(\partial_j - \frac{Z_j^n}{Z_n^n} \partial_n \right)} \phi$$

must be dominated by behaviour of Z_i^n / Z_n^n terms in the limit of large Z , and not by the derivatives of ϕ . One practical consequence would be that for points Z with large $\|Z\|$ but small Z_i for some i , the flat metric along the direction i looks like the Fubini–Study metric. This is consistent with our other observations, and also appears linked to Conjecture 6.1.

These statements and conjectures point to a deeper pattern in the structure of ϕ that we do not yet capture. We plan to revisit this curious behaviour in future work, and hope that by studying it we will learn more about properties of the Calabi–Yau flat metric.

6.1 Exact Formulae for the Flat Metric

In Section 5 we described how to find approximate expressions for ϕ . Now, we ask if it is also possible to produce *exact* formulae for the flat metric. To begin our search, we make the following assumption:

Assumption 6.1. *The flat metric may either be a closed form expression or an infinite series, but all numbers appearing in it must be computable up to a shared constant multiplicative factor.*

By a *computable number*, we mean that it can be independently computed to arbitrary precision and is not a result of, e.g., least squares regression on the formula. The flat metric is only unique up to scaling and we have to provision for this free factor in our assumption.

Assumption 6.1 is strong and rules out all approximations from the previous section, meaning that a different approach is needed here. Due to the complexity of this problem, we do not hope to find a formula for the metric that works globally. Instead, we focus on specific loci where such a formula may be easier to find, such as the pseudo-origin $(1, \sqrt[n+1]{-1}, 0, \dots, 0)$ and the equimodular locus defined by $|Z_1| = |Z_2| = \dots = |Z_n|$.

Proposition 6.4. *On a pseudo-origin of the Fermat Calabi–Yau, the flat metric g_b , with the same volume as g_{FS} satisfies*

$$g_b|_{(1, \sqrt[n+1]{-1}, 0, \dots, 0)} = \lambda I$$

where $\lambda = (\kappa/(n+1)^2)^{1/(n-1)}$, κ is the normalisation constant defined in Eq. (2.5) and I is the identity matrix.

Proof. Consider the isometry generated by toric symmetries, and its associated Jacobian $J = \text{diag}(e^{\frac{2a_k i\pi}{n+1}})$ for arbitrary $a_k \in \mathbb{Z}$. Since the pseudo-origin is a fixed point of this isometry, we have $g_b = Jg_b J^\dagger$. This must hold for any choice of a_k , but one can show that this is possible only if g_b is a purely diagonal matrix here. Then, due to permutation symmetry, we deduce that it must be a scalar multiple of the identity matrix. The precise coefficient λ is then derived from $\det g_b = \kappa|\Omega|^2$, because right-hand side simplifies to $\kappa/(n+1)^2$ on the pseudo-origin. \square

Proposition 6.5. *Assume Conjecture 3.2. Then, the flat metric g_b of a Fermat Calabi–Yau with the same volume as g_{FS} , when restricted to the equimodular locus X , satisfies*

$$g_b|_X = (n+1)\pi\lambda^* g_{\text{FS}}$$

Proof. Assuming that ϕ functionally depends only on absolute values, and applying the chain rule and permutation symmetry, we obtain $\partial\bar{\partial}\phi|_X = aI + bZ^\dagger \otimes Z$. We obtain the desired expression by substituting this into $\det g_b = \kappa|\Omega|^2$ and following a derivation analogous to Lemma A.3. \square

These propositions are significant because they give direct formulae for the elusive flat metric. The first is proven directly for a pseudo-origin of the Fermat Calabi–Yau, while the second requires our symmetry assumptions. Still, the second proposition is much stronger,

as it says that we can fully describe the flat metric on a subspace of dimension approximately half that of the Calabi–Yau.

The coefficient λ plays the role of the free parameter in these equations, since λ is precisely derived from fixing the volume of the metric. It is also noteworthy how cleanly this parameter is shared between the formulae, and that fixing the volume affects both formulae in *exactly the same way*.

In addition to these two statements, we also present these conjectures about g_b and ϕ :

Conjecture 6.6. *On a Fermat Calabi–Yau of dimension $d > 1$, only the pseudo-origins and the equimodular locus satisfy the equation*

$$g_b = \left(\frac{\det g_b}{\det \iota^* g_{\text{FS}}} \right)^{1/(n-1)} \iota^* g_{\text{FS}}$$

One can check that this equation is consistent with both Propositions 6.4 and 6.5.

Furthermore, it can be used to approximate the flat metric of nearby points due to continuity, but we cannot stretch this too far. Firstly, the formula is not Kähler in higher dimensions, so it cannot work globally except in dimension 1 where it is trivially true for any Calabi–Yau. Secondly, the formula only provides solid estimate close to the equimodular locus and pseudo-origins. For example, on the Quintic, on a dataset of 15000 points where all absolute values are within 10% of each other ($\min|Z_i|/\max|Z_i| > 0.9$), we compute that the relative error $\|g_b - g_{\text{approx}}\|_F/\|g_b\|_F$ never exceeds 6%, with a mean of just 2%, where $\|\cdot\|_F$ is the Frobenius norm.

On the other hand, far away from the equimodular locus the error increases to 42%. It is interesting that this error does not diverge globally even though it does not have a theoretically guaranteed upper bound, suggesting that this approximation performs better than a random expression would. Specifically, it performs better than a simpler estimate $g_b \approx \iota^* g_{\text{FS}}$, for which the relative error reaches 79% globally.

Still, there are better ways to generalise Propositions 6.4 and 6.5, and in a way that at least produces Kähler metrics. We can take the previously established relation $\phi \approx \sqrt{\alpha s_2}$ and solve for α on the pseudo-origin.

Proposition 6.7. *A potential $\phi = \sqrt{\alpha s_2}$ yields the metric $(\frac{1}{2\pi} - \frac{\sqrt{2}}{4}\alpha)I$ on the pseudo-origin. Thus, the choice of α that yields the flat metric on the pseudo-origin is $\alpha = \sqrt{2}(\frac{1}{\pi} - 2\lambda)$.*

Here, λ again equals $(\kappa/(n+1)^2)^{1/(n-1)}$. Curiously, $\phi = (\frac{1}{\pi} - 2\lambda)\sqrt{2s_2}$ reduces the σ -measure compared to the Fubini–Study metric on the *entire* Calabi–Yau, even though it was fit to produce flat metric only on a set of isolated points. We plot the performance of this formula as $(\dots)\sqrt{s_2}$ in Fig. 12.

7 Discussion

This paper seeks to shed light on the underlying analytic form for the Kähler potential of a Ricci-flat metric over a Calabi–Yau manifold. This is typically considered to be a “complicated non-holomorphic function” [36].

Our main contributions are as follows. We develop a novel approach for analysing numerical flat metric approximations, with a specific focus on Fermat manifolds due to their highly symmetric nature. We show that saliencies of neural network approximations yield new insights into symmetries of the flat metric of these manifolds. We pursue the theoretical aspect of this result and formulate a criterion for when the flat metric admits a representation in terms of fewer parameters than previously thought. The criterion concerns the symmetry group of ϕ when extended to the ambient space, and in particular says that if the only monomial in Q containing some Z_i is Z_i^{n+1} , then ϕ depends only on $|Z_i|$ and not on $\arg Z_i$. We also explore practical consequences of this, and use our criterion to greatly enhance neural network performance by reducing training time and memory cost, while increasing accuracy.

Specifically, we demonstrate that isometries of Fermat Calabi–Yaus can always be encoded into NN models using Graph Neural Networks and a carefully chosen set of features that are invariant to these isometries. However, we also show that our criterion allows us to create ModNet, an even simpler model that converges to state-of-the-art loss on Fermat manifolds after training for just one epoch. This calls for a deeper investigation into the criterion (Conjecture 3.2), since it has substantial experimental support despite being left unproved. If this conjecture can be falsified, it would imply that some features have a large impact on the flat metric, while others have a proportionally very small yet non-zero impact. This hierarchy problem would then require a theoretical explanation, and would have practical consequences for approximating flat metrics. This is evidenced by our state-of-the-art model, ModNet, which outperforms more general neural networks while using only a limited set of features.

In the second half of the paper we treat the flat metrics with symbolic methods. Through a combination of symbolic regression, least-squares fitting, and our own intuition, we distill our neural nets into short closed-form approximations with no increase in loss. These expressions have up to 2000x less parameters than the models they were distilled from (Fig. 12), and orders of magnitude less than the Hermitian matrix in the Donaldson’s algorithm [2].

Crucially, our results are *generalisable*. All of our conjectures (Section 3.3), observations (Section 4), symbolic constructions (Sections 5 and 6.1), etc., hold equally well on every Calabi–Yau in the Fermat family that we tested, from the complex torus to the sextic. The consistency of our results rules out the chance that they are one-off coincidences. This motivates further study of these manifolds as a unified family with shared properties, rather than taking the more common approach of only looking at deformations of a Calabi–Yau in a single dimension. Furthermore, even though we give formulae for Fermat Calabi–Yaus only, they can be constructed for other symmetric hypersurfaces too, as their only precursor is using Conjecture 3.2 to reduce the search space.

Finally, we use our high-quality approximations to propose a variety of novel statements about the flat metrics. We show that our flat metric approximation is very close to satisfying $c_3 \leq 0$ where c_3 is the third Chern class, which could be an early sign of a new Bogomolov–Yau-type inequality for c_3 . We also show that our proposed constraints for the flat metric are sufficient to yield an exact solution on several loci on Fermat manifolds. In this way we

again demonstrate the strength of our symmetry arguments.

In conclusion, our results are relevant both to algebraic geometry, by showing how Explainable AI produces new insights into properties of Calabi–Yau flat metrics, and to string phenomenology, by showing that it is possible for the flat metrics to be both highly accurate and interpretable. This paper barely scratches the surface of the consequences of our symmetry arguments, and we hope to inspire future work that will enable a better understanding of the flat metrics and the symmetries thereof.

Acknowledgments

We wish to thank Daattavya Aggrawal, Per Berglund, Carl Henrik Ek, Mario Garcia-Fernandez, Tristan Hübsch, Ferenc Huszár, Vishnu Jejjala, Oisin Kim and Pietro Liò for helpful conversations. We also thank Justin Tan for his valuable comments and assistance with the benchmarking process. Part of this work was supported by a Turing AI World-Leading Researcher Fellowship G111021. Viktor Mirjanic is supported by a Trinity College studentship. Challenger Mishra is supported by the Accelerate Program for Scientific Discovery.

A Theorem Proofs

Lemma A.1. *An invertible matrix A and vectors u, v satisfy*

$$\det(A + uv^\dagger) = (1 + v^\dagger A^{-1}u) \det(A) \quad (\text{Matrix Determinant Lemma})$$

$$(A + uv^\dagger)^{-1} = A^{-1} - \frac{A^{-1}uv^\dagger A^{-1}}{1 + v^\dagger A^{-1}u} \quad (\text{Sherman-Morrison Formula})$$

Lemma A.2 (Euler’s Homogeneous Function Theorem). *An n -th degree homogeneous function u satisfies*

$$\sum_i Z_i \frac{\partial u}{\partial Z_i} = nu$$

Lemma A.3 (Pullback of Fubini Study Identity). *Suppose u is a $(0, 0)$ -form of degree $n + 1$ on \mathbb{P}^n and let ι^* be the pullback to the variety defined by $u = 0$. Then, on a patch where $Z_0 = 1$, and where we eliminate Z_n via u to obtain local coordinates z , we have*

$$\det \iota^* g_{\text{FS}} = \frac{\|\nabla u\|^2}{\left| \frac{\partial u}{\partial Z_n} \right|^2 (1 + \|z\|^2)^n}$$

Proof. First, define $u_i = \partial u / \partial Z_i$. Then, define the pullback matrix J of ι^* as

$$J = \begin{pmatrix} 1 & \dots & 0 & -u_1/u_n \\ \vdots & \ddots & \vdots & \vdots \\ 0 & \dots & 1 & -u_{n-1}/u_n \end{pmatrix}_{(n-1) \times n}$$

and write $\iota^* g_{\text{FS}} = J g_{\text{FS}} J^\dagger$. The main difficulty is in that J is not square, so $\det \iota^* g_{\text{FS}} \neq |\det J|^2 \det g_{\text{FS}}$. Instead, we use the matrix determinant lemma and Sherman-Morrison to obtain

$$\det(JJ^\dagger) = \det\left(I + \frac{u_{1:n-1} u_{1:n-1}^\dagger}{|u_n|^2}\right) = 1 + \frac{\sum_{i=1}^{n-1} |u_i|^2}{|u_n|^2} = \frac{\|u_{1:n}\|^2}{|u_n|^2}$$

$$J^\dagger (JJ^\dagger)^{-1} J = J^\dagger \left(I + \frac{u_{1:n-1} u_{1:n-1}^\dagger}{|u_n|^2 + u_{1:n-1}^\dagger u_{1:n-1}}\right) J = I - \frac{u_{1:n} u_{1:n}^\dagger}{\|u_{1:n}\|^2}$$

where we use $u_{a:b}$ to specify a range of values in u . Finally, we compute

$$\begin{aligned} \det \iota^* g_{\text{FS}} &= \det(J g_{\text{FS}} J^\dagger) && \text{substitute } \iota^* \\ &= \det\left(J \left(\frac{1}{1 + \|z\|^2} I - \frac{z^\dagger \otimes z}{(1 + \|z\|^2)^2}\right) J^\dagger\right) && \text{substitute } g_{\text{FS}} \\ &= \frac{1}{(1 + \|z\|^2)^{n-1}} \det\left(J J^\dagger - \frac{(J z^\dagger)(z J^\dagger)}{1 + \|z\|^2}\right) && \text{rearrange} \\ &= \frac{1}{(1 + \|z\|^2)^{n-1}} \left(1 - \frac{z J^\dagger (J J^\dagger)^{-1} J z^\dagger}{1 + \|z\|^2}\right) \det(J J^\dagger) && \text{matrix det lemma} \\ &= \frac{\|u_{1:n}\|^2}{|u_n|^2 (1 + \|z\|^2)^{n-1}} \left(1 - \frac{z J^\dagger (J J^\dagger)^{-1} J z^\dagger}{1 + \|z\|^2}\right) && \text{substitute } \det(J J^\dagger) \\ &= \frac{\|u_{1:n}\|^2}{|u_n|^2 (1 + \|z\|^2)^{n-1}} \left(1 - \frac{z \left(\|u_{1:n}\|^2 I - u_{1:n} u_{1:n}^\dagger\right) z^\dagger}{\|u_{1:n}\|^2 (1 + \|z\|^2)}\right) && \text{substitute } J^\dagger (J J^\dagger)^{-1} J \\ &= \frac{\|u_{1:n}\|^2}{|u_n|^2 (1 + \|z\|^2)^{n-1}} \frac{\|u_{1:n}\|^2 + |z_{1:n} u_{1:n}|^2}{\|u_{1:n}\|^2 (1 + \|z\|^2)} && \text{simplify } (-) \\ &= \frac{\|u_{1:n}\|^2 + |z_{1:n} u_{1:n}|^2}{|u_n|^2 (1 + \|z\|^2)^n} && \text{factor} \\ &= \frac{\|u_{1:n}\|^2 + |(n+1)u - u_0|^2}{|u_n|^2 (1 + \|z\|^2)^{n-1}} && \text{Euler} \\ &= \frac{\|u_{1:n}\|^2 + |u_0|^2}{|u_n|^2 (1 + \|z\|^2)^n} && \text{substitute } u = 0 \\ &= \frac{\|\nabla u\|^2}{\left|\frac{\partial u}{\partial Z_n}\right|^2 (1 + \|z\|^2)^n} && \text{introduce } \nabla u \end{aligned}$$

which completes the proof. \square

Theorem A.4 (Integration Weights Identity). *On a Calabi–Yau in \mathbb{P}^n with a defining polynomial Q , the integration weights are explicitly*

$$w = \frac{\|Z\|^{2n}}{\|\nabla Q\|^2}$$

Proof. From Lemma A.3 we have

$$\det \iota^* g_{\text{FS}} = \frac{\|\nabla Q\|^2}{\left| \frac{\partial Q}{\partial Z_n} \right|^2 (1 + \|z\|^2)^n}$$

since Q is homogeneous. We also know that

$$\det g_b = \frac{1}{\left| \frac{\partial Q}{\partial Z_n} \right|^2}$$

Taking the fraction and setting $\|Z\|^2 = 1 + \|z\|^2$ completes the proof. \square

B Low Loss Coefficients

In Section 5 we introduced the formula

$$\hat{\phi} \approx \sum_i \sum_j c_{ij} n+1 \sqrt{s_i}^j$$

that not only approximates $\hat{\phi}$ well, but simultaneously achieves low σ -loss. Here we present exact coefficients computed with the least squares method.

Observe how the coefficients are spanning several orders of magnitude. Also, note that the results are quite sensitive to the precision of c_{ij} , and that truncating them increases loss.

Table 5. Coefficients c_{ij} for the torus ($d = 1$), achieving $\mathcal{L}_\sigma = 3.6 \times 10^{-5}$

i	j		
	1	2	3
2	0.001 515 09	0.101 742 07	-0.028 501 38
3	0.000 291 61	0.012 533 20	-0.004 502 05
4	-0.000 698 93	-0.016 215 88	0.002 290 31

Table 6. Coefficients c_{ij} for the quintic ($d = 3$), achieving $\mathcal{L}_\sigma = 0.0011$

i	j			
	1	2	3	4
2	$4.794\ 19 \times 10^{-1}$	$-6.119\ 43 \times 10^{-1}$	$5.605\ 22 \times 10^{-1}$	$-1.846\ 79 \times 10^{-1}$
3	$6.507\ 26 \times 10^{-2}$	$2.395\ 88 \times 10^{-2}$	$1.790\ 43 \times 10^{-4}$	$-5.575\ 22 \times 10^{-4}$
4	$-7.716\ 05 \times 10^{-5}$	$4.158\ 51 \times 10^{-2}$	3.7261×10^{-3}	$-1.729\ 34 \times 10^{-2}$
5	$-2.465\ 64 \times 10^{-2}$	$-2.900\ 67 \times 10^{-2}$	$2.200\ 76 \times 10^{-2}$	$1.579\ 47 \times 10^{-2}$
6	$1.905\ 15 \times 10^{-2}$	$-7.084\ 50 \times 10^{-3}$	$3.457\ 97 \times 10^{-5}$	$-5.417\ 03 \times 10^{-2}$

C Generating Interpretable Formulae with PySR

We attempted to use PySR by Cranmer [51] in two different ways to find symbolic flat metrics.

Firstly, we tried to learn symbolic $\hat{\phi}$ in the standard knowledge distillation setup, where a pretrained MLP would act as the teacher, and PySR would be the student learning to approximate ϕ . While PySR did find formulae that minimised the surrogate MSE loss on $\hat{\phi}$, these formulae did not minimise the underlying σ -loss on \hat{g} , so we abandoned this approach.[‡]

Secondly, we attempted to learn symbolic $\hat{\phi}$ in an “end-to-end” fashion, by writing a custom Julia loss function that directly minimises the σ -loss, and therefore bypassing the student-teacher setup and the misalignment between approximations of ϕ and g .

This worked better, and we obtained several symbolic approximations on the torus (Table 7). These formulae were found using a dataset of **just 300 points**, versus 10^7 used in ML, demonstrating the strength of the simplicity bias that PySR offers. In particular, note that the last formula has loss comparable to the one found in Section 5.1.

Table 7. Symbolic formulae for ϕ on the Complex Torus as discovered with PySR, and their associated σ -losses. The coefficients were slightly cleaned by hand. Note that s_2 alone is not enough to minimise σ -loss.

Symbolic $\hat{\phi}$	\mathcal{L}_σ
$0.0751 \times s_2$	0.0038
$0.0804 \times s_2^{\frac{3}{4}}$	7.6449×10^{-4}
$0.0961 \times s_2 \left(\frac{3}{4}\right)^{s_2}$	7.5138×10^{-4}
$(0.00501 + 0.01102 \times s_2 - 0.00157 \times s_3)^{\frac{1}{\pi}}$	4.4357×10^{-5}

However, this approach proved impossible to scale to higher dimensions due to differentiation bottlenecks in Julia code, so we could not test this for dimensions $d > 1$. As for the formulae themselves, only the last one in Table 7 makes sense to generalise, and we observe that the generalisations work reasonably well.

D Feature Attribution on the Quintic

See Fig. 14.

[‡]Do not forget that the σ -loss is itself a surrogate loss for the true Ricci loss, and alignment between those two is a problem of its own [33, 34].

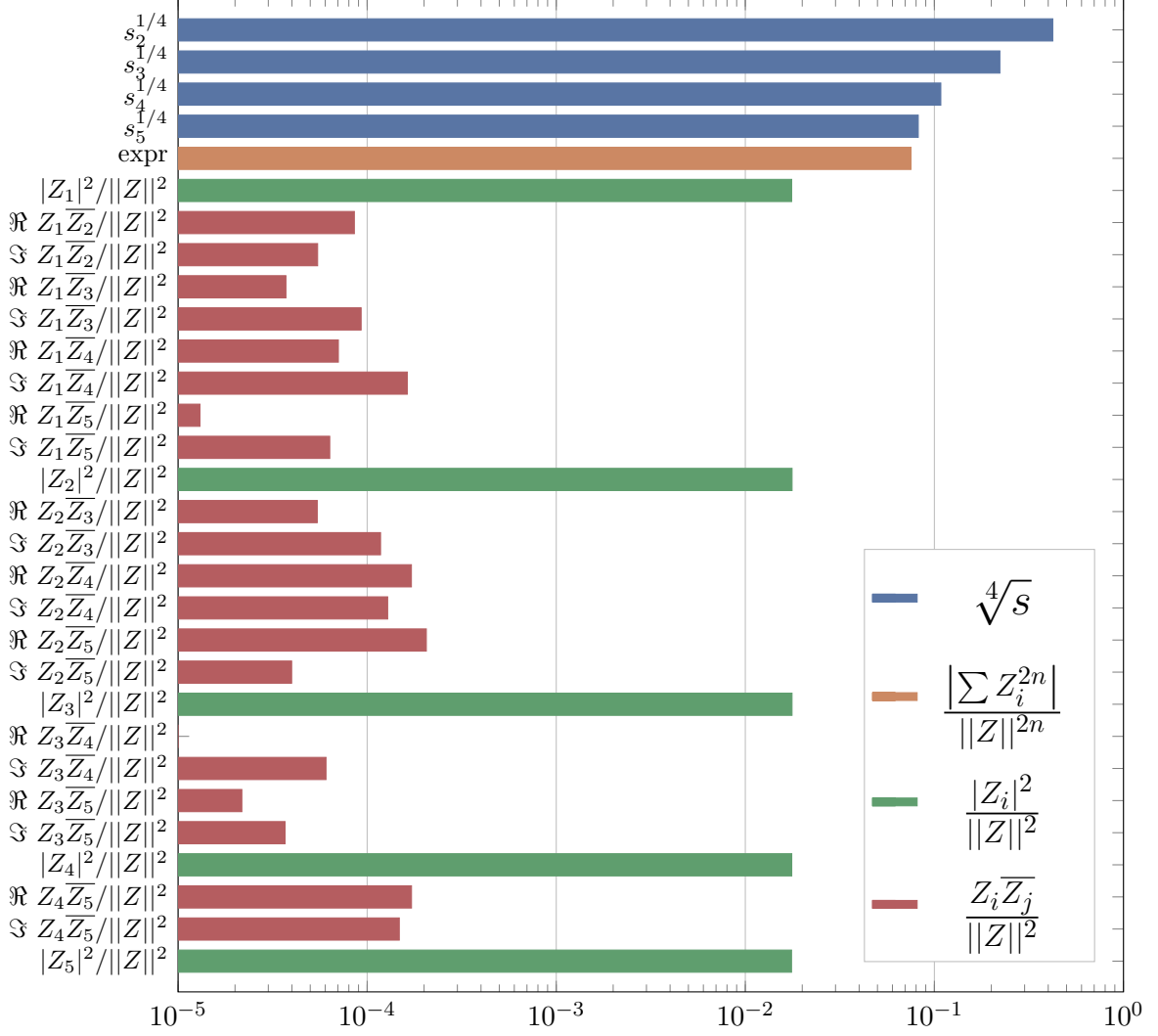


Figure 14. Normalised attribution weights a on the quintic displayed on the log scale, computed by averaging over 2×10^5 points.

E Second Order Differentiation Lemma

Lemma E.1 (Chain Rule for Second-Order Mixed Wirtinger Derivatives). *Let $f : \mathbb{C}^n \rightarrow \mathbb{R}^m$ and $g : \mathbb{R}^m \rightarrow \mathbb{R}$ be functions such that*

$$\begin{aligned} z &= (z_1, \dots, z_n) \in \mathbb{C}^n \\ f(z, \bar{z}) &= (f_1, \dots, f_m) \\ h(z, \bar{z}) &= g(f(z, \bar{z})) \end{aligned}$$

Then, for any $j, k = 1, \dots, n$, the second-order mixed Wirtinger derivative of h is given by:

$$\frac{\partial^2 h}{\partial z_j \partial \bar{z}_k} = \sum_{i=1}^m \sum_{l=1}^m \frac{\partial^2 g}{\partial f_i \partial f_l} \frac{\partial f_i}{\partial z_j} \frac{\partial f_l}{\partial \bar{z}_k} + \sum_{i=1}^m \frac{\partial g}{\partial f_i} \frac{\partial^2 f_i}{\partial z_j \partial \bar{z}_k} \quad (\text{E.1})$$

References

- [1] Shing-Tung Yau. “On the ricci curvature of a compact kähler manifold and the complex monge-ampère equation, I”. en. In: *Communications on Pure and Applied Mathematics* 31.3 (1978), pp. 339–411. ISSN: 1097-0312. DOI: [10.1002/cpa.3160310304](https://doi.org/10.1002/cpa.3160310304).
- [2] S. K. Donaldson. “Some Numerical Results in Complex Differential Geometry”. EN. In: *Pure and Applied Mathematics Quarterly* 5.2 (2005), pp. 571–618. ISSN: 1558-8602. DOI: [10.4310/PAMQ.2009.v5.n2.a2](https://doi.org/10.4310/PAMQ.2009.v5.n2.a2).
- [3] Carl Henrik Ek, Oisin Kim, and Challenger Mishra. *Calabi-Yau metrics through Grassmannian learning and Donaldson’s algorithm*. Oct. 2024.
- [4] Philip Candelas et al. “A pair of Calabi-Yau manifolds as an exactly soluble superconformal theory”. In: *Nuclear Physics B* 359.1 (July 1991), pp. 21–74. ISSN: 0550-3213. DOI: [10.1016/0550-3213\(91\)90292-6](https://doi.org/10.1016/0550-3213(91)90292-6).
- [5] Volker Braun et al. “Calabi-Yau metrics for quotients and complete intersections”. en. In: *Journal of High Energy Physics* 2008.05 (May 2008), pp. 080–080. ISSN: 1029-8479. DOI: [10.1088/1126-6708/2008/05/080](https://doi.org/10.1088/1126-6708/2008/05/080).
- [6] V. Braun, P. Candelas, and R. Davies. “A three-generation Calabi-Yau manifold with small Hodge numbers”. en. In: *Fortschritte der Physik* 58.4-5 (2010), pp. 467–502. ISSN: 1521-3978. DOI: [10.1002/prop.200900106](https://doi.org/10.1002/prop.200900106).
- [7] Rhys Davies. “Calabi-Yau threefolds and heterotic string compactification”. PhD Thesis. Oxford U., 2010.
- [8] Volker Braun. “On free quotients of complete intersection Calabi-Yau manifolds”. en. In: *Journal of High Energy Physics* 2011.4 (Apr. 2011), p. 5. ISSN: 1029-8479. DOI: [10.1007/JHEP04\(2011\)005](https://doi.org/10.1007/JHEP04(2011)005).
- [9] C. Mishra. “Calabi-Yau manifolds, discrete symmetries and string theory”. English. PhD Thesis. University of Oxford, 2017.
- [10] Philip Candelas, Andrei Constantin, and Challenger Mishra. “Calabi-Yau Threefolds with Small Hodge Numbers”. en. In: *Fortschritte der Physik* 66.6 (2018), p. 1800029. ISSN: 1521-3978. DOI: [10.1002/prop.201800029](https://doi.org/10.1002/prop.201800029).
- [11] Andre Lukas and Challenger Mishra. “Discrete Symmetries of Complete Intersection Calabi–Yau Manifolds”. en. In: *Communications in Mathematical Physics* 379.3 (Nov. 2020), pp. 847–865. ISSN: 1432-0916. DOI: [10.1007/s00220-020-03838-6](https://doi.org/10.1007/s00220-020-03838-6).
- [12] Lara Briana Anderson. “Heterotic and M-theory compactifications for string phenomenology”. eng. PhD thesis. University of Oxford, 2008.
- [13] Andrei Constantin et al. *Fermion Masses and Mixing in String-Inspired Models*. en. Oct. 2024. DOI: [10.48550/arXiv.2410.17704](https://doi.org/10.48550/arXiv.2410.17704).
- [14] Luis E Ibanez and Graham G Ross. “Discrete gauge symmetries and the origin of baryon and lepton number conservation in supersymmetric versions of the standard model”. In: *Nuclear Physics B* 368.1 (1992), pp. 3–37.

- [15] P. Candelas and R. Davies. “New Calabi-Yau manifolds with small Hodge numbers”. en. In: *Fortschritte der Physik* 58.4-5 (2010), pp. 383–466. ISSN: 1521-3978. DOI: [10.1002/prop.200900105](https://doi.org/10.1002/prop.200900105).
- [16] Philip Candelas and Challenger Mishra. “Highly Symmetric Quintic Quotients”. en. In: *Fortschritte der Physik* 66.4 (2018), p. 1800017. ISSN: 1521-3978. DOI: [10.1002/prop.201800017](https://doi.org/10.1002/prop.201800017).
- [17] Philip Candelas, Andrei Constantin, and Challenger Mishra. “Hodge numbers for CICYs with symmetries of order divisible by 4”. In: *Fortschritte der Physik* 64.6-7 (2016), pp. 463–509.
- [18] Andrei Constantin, Andre Lukas, and Challenger Mishra. “The family problem: hints from heterotic line bundle models”. In: *Journal of High Energy Physics* 2016.3 (2016), pp. 1–17.
- [19] Vishnu Jejjala, Damián Kaloni Mayorga Peña, and Challenger Mishra. “Neural network approximations for Calabi-Yau metrics”. en. In: *Journal of High Energy Physics* 2022.8 (Aug. 2022), p. 105. ISSN: 1029-8479. DOI: [10.1007/JHEP08\(2022\)105](https://doi.org/10.1007/JHEP08(2022)105).
- [20] Michael M. Bronstein et al. *Geometric Deep Learning: Grids, Groups, Graphs, Geodesics, and Gauges*. May 2021.
- [21] G. Cybenko. “Approximation by superpositions of a sigmoidal function”. en. In: *Mathematics of Control, Signals and Systems* 2.4 (Dec. 1989), pp. 303–314. ISSN: 1435-568X. DOI: [10.1007/BF02551274](https://doi.org/10.1007/BF02551274).
- [22] Kurt Hornik, Maxwell Stinchcombe, and Halbert White. “Multilayer feedforward networks are universal approximators”. In: *Neural Networks* 2.5 (Jan. 1989), pp. 359–366. ISSN: 0893-6080. DOI: [10.1016/0893-6080\(89\)90020-8](https://doi.org/10.1016/0893-6080(89)90020-8).
- [23] Kurt Hornik. “Approximation capabilities of multilayer feedforward networks”. In: *Neural Netw.* 4.2 (Mar. 1991), pp. 251–257. ISSN: 0893-6080. DOI: [10.1016/0893-6080\(91\)90009-T](https://doi.org/10.1016/0893-6080(91)90009-T).
- [24] Keyulu Xu et al. *How Powerful are Graph Neural Networks?* en. Feb. 2019.
- [25] Maziar Raissi, Paris Perdikaris, and George Em Karniadakis. *Physics Informed Deep Learning (Part I): Data-driven Solutions of Nonlinear Partial Differential Equations*. en. Nov. 2017.
- [26] M. Raissi, P. Perdikaris, and G. E. Karniadakis. “Physics-informed neural networks: A deep learning framework for solving forward and inverse problems involving nonlinear partial differential equations”. In: *Journal of Computational Physics* 378 (Feb. 2019), pp. 686–707. ISSN: 0021-9991. DOI: [10.1016/j.jcp.2018.10.045](https://doi.org/10.1016/j.jcp.2018.10.045).
- [27] P. Candelas et al. “Vacuum configurations for superstrings”. In: *Nuclear Physics B* 258 (Jan. 1985), pp. 46–74. ISSN: 0550-3213. DOI: [10.1016/0550-3213\(85\)90602-9](https://doi.org/10.1016/0550-3213(85)90602-9).
- [28] Frederik Denef and Michael R. Douglas. “Distributions of flux vacua”. In: *Journal of High Energy Physics* 2004.05 (May 2004), pp. 072–072. ISSN: 1029-8479. DOI: [10.1088/1126-6708/2004/05/072](https://doi.org/10.1088/1126-6708/2004/05/072).

- [29] Philip Candelas and Xenia de la Ossa. *Lectures on Complex Manifolds*. Aug. 1987.
- [30] Tristan Hübsch. *Calabi-Yau Manifolds: A Bestiary for Physicists*. en. World Scientific, 1994. ISBN: 978-981-02-1927-7.
- [31] Michael R. Douglas et al. “Numerical Calabi-Yau metrics”. In: *Journal of Mathematical Physics* 49.3 (Mar. 2008), p. 032302. ISSN: 0022-2488, 1089-7658. DOI: [10.1063/1.2888403](https://doi.org/10.1063/1.2888403).
- [32] Michael R. Douglas et al. “Numerical solution to the hermitian Yang-Mills equation on the Fermat quintic”. en. In: *Journal of High Energy Physics* 2007.12 (Dec. 2007), pp. 083–083. ISSN: 1029-8479. DOI: [10.1088/1126-6708/2007/12/083](https://doi.org/10.1088/1126-6708/2007/12/083).
- [33] Magdalena Larfors et al. *Learning Size and Shape of Calabi-Yau Spaces*. Nov. 2021.
- [34] Yacoub Hendi, Magdalena Larfors, and Moritz Walden. *Learning Group Invariant Calabi-Yau Metrics by Fundamental Domain Projections*. en. July 2024.
- [35] Per Berglund et al. *Machine Learned Calabi-Yau Metrics and Curvature*. Feb. 2023. DOI: [10.48550/arXiv.2211.09801](https://doi.org/10.48550/arXiv.2211.09801).
- [36] Anthony Ashmore, Yang-Hui He, and Burt Ovrut. “Machine learning Calabi-Yau metrics”. In: *Fortschritte der Physik* 68.9 (Sept. 2020), p. 2000068. ISSN: 0015-8208, 1521-3978. DOI: [10.1002/prop.202000068](https://doi.org/10.1002/prop.202000068).
- [37] Mathis Gerdes and Sven Krippendorf. *CYJAX: A package for Calabi-Yau metrics with JAX*. Nov. 2022. DOI: [10.48550/arXiv.2211.12520](https://doi.org/10.48550/arXiv.2211.12520).
- [38] Matthew Headrick and Ali Nassar. *Energy functionals for Calabi-Yau metrics*. Feb. 2010.
- [39] Matthew Headrick and Toby Wiseman. “Numerical Ricci-flat metrics on K3”. en. In: *Classical and Quantum Gravity* 22.23 (Dec. 2005), pp. 4931–4960. ISSN: 0264-9381, 1361-6382. DOI: [10.1088/0264-9381/22/23/002](https://doi.org/10.1088/0264-9381/22/23/002).
- [40] Lara B. Anderson, James Gray, and Magdalena Larfors. *Lectures on Numerical and Machine Learning Methods for Approximating Ricci-flat Calabi-Yau Metrics*. Dec. 2023. DOI: [10.48550/arXiv.2312.17125](https://doi.org/10.48550/arXiv.2312.17125).
- [41] Giorgi Butbaia et al. *Physical Yukawa Couplings in Heterotic String Compactifications*. May 2024. DOI: [10.48550/arXiv.2401.15078](https://doi.org/10.48550/arXiv.2401.15078).
- [42] Edward Witten. “Symmetry breaking patterns in superstring models”. In: *Nuclear Physics B* 258 (Jan. 1985), pp. 75–100. ISSN: 0550-3213. DOI: [10.1016/0550-3213\(85\)90603-0](https://doi.org/10.1016/0550-3213(85)90603-0).
- [43] Lara B. Anderson et al. “Moduli-dependent Calabi-Yau and SU(3)-structure metrics from machine learning”. en. In: *Journal of High Energy Physics* 2021.5 (May 2021), p. 13. ISSN: 1029-8479. DOI: [10.1007/JHEP05\(2021\)013](https://doi.org/10.1007/JHEP05(2021)013).
- [44] Wilhelm Karl Joseph Killing. *Die nicht-euklidischen Raumformen in analytischer Behandlung*. ger. Leipzig B.G. Teubner, 1885.

- [45] Shamit Kachru, Arnav Tripathy, and Max Zimet. *K3 metrics*. Oct. 2020. DOI: [10.48550/arXiv.2006.02435](https://doi.org/10.48550/arXiv.2006.02435).
- [46] Per Berglund et al. *cymc – Calabi-Yau Metrics, Yukawas, and Curvature*. Oct. 2024. DOI: [10.48550/arXiv.2410.19728](https://doi.org/10.48550/arXiv.2410.19728).
- [47] Ziming Liu et al. *KAN: Kolmogorov-Arnold Networks*. June 2024. DOI: [10.48550/arXiv.2404.19756](https://doi.org/10.48550/arXiv.2404.19756).
- [48] A. K. Kolmogorov. “On the Representation of Continuous Functions of Several Variables by Superposition of Continuous Functions of One Variable and Addition”. In: *Doklady Akademii Nauk SSSR* 114 (1957), pp. 369–373.
- [49] “Representation of continuous functions of three variables by the superposition of continuous functions of two variables”. en. In: *Collected Works: Representations of Functions, Celestial Mechanics and KAM Theory, 1957–1965*. Ed. by Vladimir I. Arnold et al. Berlin, Heidelberg: Springer, 2009, pp. 47–133. ISBN: 978-3-642-01742-1. DOI: [10.1007/978-3-642-01742-1_6](https://doi.org/10.1007/978-3-642-01742-1_6).
- [50] Miles Cranmer et al. “Discovering Symbolic Models from Deep Learning with Inductive Biases”. In: *NeurIPS 2020* (2020). arXiv: [2006.11287](https://arxiv.org/abs/2006.11287) [cs.LG].
- [51] Miles Cranmer. *Interpretable Machine Learning for Science with PySR and SymbolicRegression.jl*. May 2023. DOI: [10.48550/arXiv.2305.01582](https://doi.org/10.48550/arXiv.2305.01582).
- [52] Mukund Sundararajan, Ankur Taly, and Qiqi Yan. “Axiomatic attribution for deep networks”. In: *Proceedings of the 34th International Conference on Machine Learning - Volume 70*. ICML’17. Sydney, NSW, Australia: JMLR.org, Aug. 2017, pp. 3319–3328.
- [53] Grégoire Montavon et al. “Layer-Wise Relevance Propagation: An Overview”. en. In: *Explainable AI: Interpreting, Explaining and Visualizing Deep Learning*. Ed. by Wojciech Samek et al. Cham: Springer International Publishing, 2019, pp. 193–209. ISBN: 978-3-030-28954-6. DOI: [10.1007/978-3-030-28954-6_10](https://doi.org/10.1007/978-3-030-28954-6_10).
- [54] Alex Davies et al. “Advancing mathematics by guiding human intuition with AI”. en. In: *Nature* 600.7887 (Dec. 2021), pp. 70–74. ISSN: 1476-4687. DOI: [10.1038/s41586-021-04086-x](https://doi.org/10.1038/s41586-021-04086-x).
- [55] Soledad Villar et al. *Scalars are universal: Equivariant machine learning, structured like classical physics*. en. Feb. 2023.
- [56] Hermann Weyl. *The Classical Groups: Their Invariants and Representations*. en. Princeton University Press, 1946. ISBN: 978-0-691-05756-9.
- [57] R. Frucht. “Herstellung von Graphen mit vorgegebener abstrakter Gruppe”. German. In: *Compositio Mathematica* 6 (1938), pp. 239–250. ISSN: 0010-437X.
- [58] Jean Gallier and Jocelyn Quaintance. “Isometries, Local Isometries, Riemannian Coverings and Submersions, and Killing Vector Fields”. en. In: *Differential Geometry and Lie Groups: A Computational Perspective*. Ed. by Jean Gallier and Jocelyn Quaintance. Cham: Springer International Publishing, 2020, pp. 541–557. ISBN: 978-3-030-46040-2. DOI: [10.1007/978-3-030-46040-2_18](https://doi.org/10.1007/978-3-030-46040-2_18).

- [59] James Bradbury et al. *JAX: composable transformations of Python+NumPy programs*. 2018.
- [60] Michael R. Douglas, Subramanian Lakshminarasimhan, and Yidi Qi. *Numerical Calabi-Yau metrics from holomorphic networks*. May 2021. DOI: [10.48550/arXiv.2012.04797](https://doi.org/10.48550/arXiv.2012.04797).
- [61] Vincent Bouchard. *Lectures on complex geometry, Calabi-Yau manifolds and toric geometry*. Feb. 2007. DOI: [10.48550/arXiv.hep-th/0702063](https://doi.org/10.48550/arXiv.hep-th/0702063).
- [62] Shing-Tung Yau. “Calabi’s conjecture and some new results in algebraic geometry”. In: *Proceedings of the National Academy of Sciences* 74.5 (May 1977), pp. 1798–1799. DOI: [10.1073/pnas.74.5.1798](https://doi.org/10.1073/pnas.74.5.1798).
- [63] F. A. Bogomolov. “Holomorphic tensors and vector bundles on projective manifolds”. In: *Izvestiya Akademii Nauk SSSR. Seriya Matematicheskaya* 42.6 (1978), pp. 1227–1287, 1439. ISSN: 0373-2436.
- [64] Fabrizio Catanese. *Kummer quartic surfaces, strict self-duality, and more*. en. May 2021. DOI: [10.48550/arXiv.2101.10501](https://doi.org/10.48550/arXiv.2101.10501).
- [65] “IEEE Standard for Floating-Point Arithmetic”. In: *IEEE Std 754-2019 (Revision of IEEE 754-2008)* (July 2019), pp. 1–84. DOI: [10.1109/IEEESTD.2019.8766229](https://doi.org/10.1109/IEEESTD.2019.8766229).